

# Charged Pion–Pair Production and Pion Polarizabilities to two Loops <sup>1</sup>

U. Bürgi

Institut für Theoretische Physik  
Universität Bern  
Sidlerstrasse 5, CH-3012 Bern, Switzerland

(e-mail: buergi@butp.unibe.ch)

July 2021

## Abstract

We evaluate the amplitude for  $\gamma\gamma \rightarrow \pi^+\pi^-$  to two loops in the framework of chiral perturbation theory. The three new coupling constants that enter the result at this order in the low-energy expansion are estimated via resonance saturation. We discuss in addition the crossed channel processes  $\gamma\pi^\pm \rightarrow \gamma\pi^\pm$  – in particular the charged pion polarizabilities – to the same accuracy. The predictions are compared with available experimental information.

---

<sup>1</sup>Work supported in part by Schweizerischer Nationalfonds

# 1 Introduction

Pion-pair production by photons at low energies may be used to test chiral perturbation theory (CHPT) [1–5]. For neutral pions, the chiral calculation at leading order – generated by one-loop diagrams [6, 7] – is not in good agreement with the available data from Crystal Ball [8] even near the threshold. Recently, the next-to-leading order contribution, generated by two-loop diagrams, has been determined in Ref. [9]. The corresponding enhancement of the cross section brings theory and experiment into agreement within the uncertainties of the calculation and the available data [9].

In the process  $\gamma\gamma \rightarrow \pi^+\pi^-$ , the Born term (that is absent in the neutral channel) dominates the behavior of the cross section at low energies. Next-to-leading corrections (one-loop graphs) change the result very little [6], and the comparison with the available data from Mark II [10] works quite well. The dispersive analysis performed in [11, 12] indicates how additional (multiloop) effects required by unitarity may influence the amplitude. The authors find only a slight change as compared to the one-loop result for center-of-mass energies  $\sqrt{s} \leq 700$  MeV. It is one of the purposes of the present article to investigate the effect of the two-loop contributions to the amplitude.

The Compton amplitude  $\gamma\pi^\pm \rightarrow \gamma\pi^\pm$  may be obtained from  $\gamma\gamma \rightarrow \pi^+\pi^-$  by crossing. The leading term in the Taylor expansion of the Compton amplitude at threshold in powers of photon energies measures the charge of the pions, whereas the next-to-leading terms are parametrized through the electric ( $\bar{\alpha}_\pi$ ) and magnetic ( $\bar{\beta}_\pi$ ) polarizabilities. These probe the rigidity of the charged pion against an external electromagnetic perturbation. At leading order in the chiral expansion, the result is [14–16]  $\bar{\alpha}_\pi = -\bar{\beta}_\pi = 2.7 \pm 0.4$ <sup>2</sup>. With the two-loop Compton amplitude at hand, it is then straightforward to evaluate  $\bar{\alpha}_\pi$  and  $\bar{\beta}_\pi$  at next-to-leading order in the quark mass expansion. The result of this analysis is presented below. Turning to the experimental aspect, we note that the experimental determination of the charged pion polarizabilities is not an easy task. At Lebedev [17] and at Serpukhov [18], relevant experiments have been performed some time ago. Unfortunately the results of these measurements do not agree very well among each other, such that a comparison with the theoretical prediction is not conclusive. In order to clarify the situation, additional experiments are planned [19].

The article is organized as follows: After setting up the kinematics and illuminating some aspects of CHPT, the effective lagrangians  $\mathcal{L}_2, \mathcal{L}_4$  and  $\mathcal{L}_6$  are discussed. For completeness we display in section 5 the tree- and one-loop result worked out earlier in [6]. We then evaluate all diagrams occurring at  $\mathcal{O}(p^6)$ , including also the pion mass and the wave function renormalization constant at two-loop order (sections 6, 7). The amplitude for  $\gamma\gamma \rightarrow \pi^+\pi^-$  is displayed in section 8, that also contains a numerical discussion of the corresponding cross section. Section 9 is devoted a discussion of Compton scattering and pion electric and magnetic polarizabilities at two-loop order. Finally, a summary and concluding remarks are given in section 10. The notation used in the text is collected in appendix A.

---

<sup>2</sup>We express the polarizabilities in units of  $10^{-4}$  fm<sup>3</sup> throughout.

## 2 Kinematics

The amplitude describing the process  $\gamma\gamma \rightarrow \pi^+\pi^-$  may be extracted from the matrix element

$$\langle \pi^+(p_1), \pi^-(p_2) \text{ out} \mid \gamma(q_1, \lambda_1), \gamma(q_2, \lambda_2) \text{ in} \rangle = i(2\pi)^4 \delta^4(P_f - P_i) T^{\gamma\gamma \rightarrow \pi^+\pi^-}, \quad (2.1)$$

where

$$\begin{aligned} T^{\gamma\gamma \rightarrow \pi^+\pi^-} &= e^2 \epsilon_1^\mu(q_1, \lambda_1) \epsilon_2^\nu(q_2, \lambda_2) W_{\mu\nu}^{\gamma\gamma \rightarrow \pi^+\pi^-}, \\ W_{\mu\nu}^{\gamma\gamma \rightarrow \pi^+\pi^-} &= i \int dx e^{-i(q_1x + q_2y)} \langle \pi^+(p_1) \pi^-(p_2) \text{ out} \mid T j_\mu(x) j_\nu(y) \mid 0 \rangle. \end{aligned} \quad (2.2)$$

$j^\mu$  denotes the electromagnetic current and  $\alpha = e^2/4\pi \simeq 1/137$  is the electromagnetic coupling. It is convenient to change the pion coordinates according to  $(\pi^\pm, \pi^0) \rightarrow (\pi^1, \pi^2, \pi^3)$  and instead of  $\pi^+\pi^-$ -production, we consider in the following the process  $\gamma\gamma \rightarrow \pi^1\pi^1$ , with

$$W_{\mu\nu}^{\gamma\gamma \rightarrow \pi^+\pi^-} = -W_{\mu\nu}^{\gamma\gamma \rightarrow \pi^1\pi^1} \doteq -V_{\mu\nu}^C, \quad (2.3)$$

where the relative minus sign stems from the Condon–Shortly phase convention. The correlator  $V_{\mu\nu}^C$  may be decomposed into four Lorentz invariant amplitudes  $A^C, B^C, C^C, D^C$  (see e.g. [9]),

$$\begin{aligned} V_{\mu\nu}^C &= A^C(s, t, u) T_{1\mu\nu} + B^C(s, t, u) T_{2\mu\nu} + C^C(s, t, u) T_{3\mu\nu} + D^C(s, t, u) T_{4\mu\nu}, \\ T_{1\mu\nu} &= \frac{s}{2} g_{\mu\nu} - q_{1\nu} q_{2\mu}, \\ T_{2\mu\nu} &= 2s \Delta_\mu \Delta_\nu - \nu^2 g_{\mu\nu} - 2\nu (q_{1\nu} \Delta_\mu - q_{2\mu} \Delta_\nu), \\ T_{3\mu\nu} &= q_{1\mu} q_{2\nu}, \\ T_{4\mu\nu} &= s (q_{1\mu} \Delta_\nu - q_{2\nu} \Delta_\mu) - \nu (q_{1\mu} q_{1\nu} + q_{2\mu} q_{2\nu}), \\ \Delta_\mu &= (p_1 - p_2)_\mu, \end{aligned} \quad (2.4)$$

where

$$\begin{aligned} s &= (q_1 + q_2)^2 = 4\vec{q}^2, \\ t &= (p_1 - q_1)^2 = M_\pi^2 - 2\vec{q}^2(1 - \beta(s) \cos \theta), \\ u &= (p_2 - q_1)^2 = M_\pi^2 - 2\vec{q}^2(1 + \beta(s) \cos \theta), \\ \nu &= t - u, \end{aligned} \quad (2.5)$$

are the standard Mandelstam variables,  $\beta(s) = (1 - 4M_\pi^2/s)^{1/2}$  is the velocity of the produced pions and  $\theta$  denotes the scattering angle,  $\vec{q}_1 \cdot \vec{p}_1 = |\vec{q}_1| |\vec{p}_1| \cos \theta$  (all quantities in the center-of-mass system). The tensor  $V_{\mu\nu}^C$  satisfies furthermore the Ward identities

$$q_1^\mu V_{\mu\nu}^C = q_2^\nu V_{\mu\nu}^C = 0. \quad (2.6)$$

The amplitudes  $A^C$  and  $B^C$  are analytic functions of the variables  $s, t$  and  $u$ , symmetric under crossing  $(t, u) \rightarrow (u, t)$ . The remaining quantities  $C^C$  and  $D^C$  do not contribute to the cross section (gauge invariance).

The differential cross section for unpolarized photons in the center-of-mass system reads with the normalization  $\langle \vec{p}_1 | \vec{p}_2 \rangle = 2(2\pi)^3 p_1^0 \delta^3(\vec{p}_1 - \vec{p}_2)$ ,

$$\begin{aligned} \frac{d\sigma^{\gamma\gamma\rightarrow\pi^+\pi^-}}{d\Omega} &= \frac{\alpha^2 s}{32} \beta(s) H^C(s, t), \\ H^C(s, t) &= |H_{++}^C|^2 + |H_{+-}^C|^2. \end{aligned} \quad (2.7)$$

Here we have introduced the helicity amplitudes  $H_{\pm\pm}^C$  corresponding to photon helicity differences  $\lambda = 0, 2$ , respectively. They are defined in terms of the amplitudes  $A^C$  and  $B^C$ ,

$$\begin{aligned} H_{++}^C &= A^C + 2(4M_\pi^2 - s)B^C, \\ H_{+-}^C &= \frac{8(M_\pi^4 - tu)}{s} B^C, \end{aligned} \quad (2.8)$$

and have partial wave expansion involving even  $J \geq \lambda$ ,

$$\begin{aligned} H_{++}^C &= \sum_{J=0,2,4,\dots} h_{C,+}^J(s) d_{00}^J(\cos\theta), \\ H_{+-}^C &= \sum_{J=2,4,6,\dots} h_{C,-}^J(s) d_{20}^J(\cos\theta). \end{aligned} \quad (2.9)$$

In the text we also use the symbols

$$\begin{aligned} \bar{H}_{++}^C &\doteq H_{++}^C - H_{B++}^C, \\ \bar{H}_{+-}^C &\doteq H_{+-}^C - H_{B+-}^C, \end{aligned} \quad (2.10)$$

where  $H_{B\pm\pm}^C$  denote the helicity amplitudes generated by the Born contributions.

For comparison with experimental results, it is convenient to present also the total cross section for the case where  $|\cos\theta|$  is less than some fixed value  $Z$ ,

$$\sigma(s, |\cos\theta| < Z) = \frac{\alpha^2 \pi}{8} \int_{t_-}^{t_+} dt H^C(s, t) \quad (2.11)$$

with

$$t_{\pm} = M_\pi^2 - 2\vec{q}^2(1 \mp \beta(s)Z). \quad (2.12)$$

### 3 Low energy expansion

We consider QCD with two flavours  $u$  and  $d$  in the isospin limit  $m_u = m_d = \hat{m}$ . Since the masses of these two quarks are small, the deviation from chiral symmetry may be studied by treating the quark mass term as a perturbation using the framework of an effective chiral lagrangian (CHPT) [1–5]. This effective lagrangian relies only on the solid assumptions of spontaneously broken  $SU(2)_L \times SU(2)_R$  chiral symmetry, Lorentz invariance and low momentum transfer. It can be expanded in a series of terms with increasing numbers of derivatives and powers of quark masses,

$$\mathcal{L}_{eff} = \mathcal{L}_2 + \mathcal{L}_4 + \mathcal{L}_6 + \dots, \quad (3.1)$$

where  $\mathcal{L}_{(2n)}$  denotes a term of order  $p^{2n}$ . Each of these terms contain a couple of monomials with couplings which are not fixed by symmetry constraints, but they are fixed by the

dynamics of the underlying theory through the renormalization group invariant scale  $\Lambda_{QCD}$  and the heavy quark masses. Up to now it has not been possible to reliably calculate them directly from the QCD lagrangian. The best way to determine their values is by comparison with experimental data. Green functions of the theory are generated by the vacuum-to-vacuum amplitude [2, 3]

$$e^{iZ(v,a,s,p)} = \langle 0_{out} | 0_{in} \rangle_{v,a,s,p} = \int [dU] e^{i \int d^4x \mathcal{L}_{eff}(U,v,a,s,p)}, \quad (3.2)$$

where the dynamical variables (pions) are contained in the matrix  $U$ . The generating functional  $Z$  admits an expansion in powers of the external momenta and the quark masses

$$Z(v, a, s, p) = Z_2 + Z_4 + Z_6 + \dots, \quad (3.3)$$

where  $Z_n$  denotes a term of order  $p^n$ . The contribution of loops to the generating functional is suppressed with respect to tree diagrams. At order  $p^2$  the contribution to the amplitude stems from  $\mathcal{L}_2$  only via tree diagrams. At next-to-leading order one has to evaluate one-loop graphs generated by  $\mathcal{L}_2$  and adding the tree graphs from  $\mathcal{L}_4$ . Diagrams at  $\mathcal{O}(p^6)$  contribute via  $Z_6$  from  $\mathcal{L}_2 + \mathcal{L}_4 + \mathcal{L}_6$  with tree, from  $\mathcal{L}_2 + \mathcal{L}_4$  with one-loop and from  $\mathcal{L}_2$  with two-loop diagrams. The one-loop diagrams at  $\mathcal{O}(p^6)$  contain one vertex from  $\mathcal{L}_4$ . We write the corresponding expansion of the amplitude as

$$I = I_2 + I_4 + I_6 + \dots, \quad I = V_{\mu\nu}^C, A^C, B^C, \quad (3.4)$$

where it is understood that  $Z_n$  generates  $I_n$ . For comprehensive reviews on chiral perturbation theory we refer the reader to [5].

## 4 The effective lagrangians $\mathcal{L}_2$ , $\mathcal{L}_4$ and $\mathcal{L}_6$

At  $\mathcal{O}(p^2)$  the most general effective lagrangian coincides with the non-linear  $\sigma$ -model lagrangian  $\mathcal{L}_2$  equipped with external fields [2],

$$\begin{aligned} \mathcal{L}_2 &= \frac{1}{4} F^2 \langle D_\mu U D^\mu U^\dagger + \chi^\dagger U + \chi U^\dagger \rangle \\ D_\mu U &= \partial_\mu U - i(v_\mu + a_\mu)U + iU(v_\mu - a_\mu), \\ \chi &= 2B(s + ip). \end{aligned} \quad (4.1)$$

The brackets  $\langle \dots \rangle$  denote a trace in flavour space and the unitary  $2 \times 2$  matrix  $U$  contains the pion fields,

$$\begin{aligned} U &= \sigma + i \frac{\phi}{F} \quad ; \quad \sigma^2 + \frac{\phi^2}{F^2} = \mathbf{1} ; \\ \phi &= \phi^i \tau^i = \begin{pmatrix} \pi^0 & \sqrt{2} \pi^+ \\ \sqrt{2} \pi^- & -\pi^0 \end{pmatrix}. \end{aligned} \quad (4.2)$$

We count the Goldstone fields as  $\mathcal{O}(p^0)$ , a derivative  $\partial_\mu$ , the vector and axial-vector currents  $v_\mu, a_\mu$  as  $\mathcal{O}(p)$  and the scalar and pseudoscalar currents  $s, p$  as  $\mathcal{O}(p^2)$ . The

lagrangian  $\mathcal{L}_2$  contains two free parameters  $F$  and  $B$ , where  $F$  is the pion decay constant in the chiral limit and  $B$  is related to the order parameter  $\langle 0 | \bar{q}q | 0 \rangle$ . In terms of physical quantities we have

$$\begin{aligned} F_\pi &= F(1 + \mathcal{O}(\hat{m})) , \\ M_\pi^2 &= M^2(1 + \mathcal{O}(\hat{m})) , \quad M^2 = 2B\hat{m}. \end{aligned} \quad (4.3)$$

The transformation properties under  $G = SU(2)_L \times SU(2)_R \times U(1)$  of the several fields are,

$$\begin{aligned} U &\rightarrow g_R U g_L^\dagger , \\ v_\mu + a_\mu &\rightarrow g_R (v_\mu + a_\mu) g_R^\dagger + i g_R \partial_\mu g_R^\dagger , \\ v_\mu - a_\mu &\rightarrow g_L (v_\mu - a_\mu) g_L^\dagger + i g_L \partial_\mu g_L^\dagger , \\ s + ip &\rightarrow g_R (s + ip) g_L^\dagger , \\ g_{L,R} &= e^{i\phi} V_{L,R} , \\ V_{L,R} &\in SU(2) ; \quad \phi = \text{diag}(\phi_0, \phi_0) ; \quad \phi \in \mathbf{R} . \end{aligned} \quad (4.4)$$

Since the charge is not a generator of  $SU(2)$ , we consider in the following the case

$$\langle a_\mu \rangle = 0 ; \quad \langle v_\mu \rangle \neq 0 . \quad (4.5)$$

This condition is consistent with the transformation law (4.4). To calculate  $V_{\mu\nu}^C$ , we set

$$s = \hat{m}\mathbf{1} ; \quad v_\mu = Q\bar{v}_\mu ; \quad p = \bar{p}^i \tau^i ; \quad a_\mu = 0 , \quad (4.6)$$

where  $Q = 1/3 \text{diag}(2, -1)$  is the charge matrix.

The next-to-leading term  $Z_4$  contains two types of contributions: one-loop graphs generated by  $\mathcal{L}_2$  and tree graphs involving one vertex from  $\mathcal{L}_4$ . The most general chiral invariant lagrangian  $\mathcal{L}_4$  was constructed by Gasser and Leutwyler [2]:

$$\begin{aligned} \mathcal{L}_4 &= \mathcal{L}^{(4)} + \mathcal{L}_{WZW} , \\ \mathcal{L}^{(4)} &= \sum_{i=1}^7 l_i P_i + \dots \end{aligned} \quad (4.7)$$

where

$$\begin{aligned} P_1 &= \frac{1}{4} \langle u^\mu u_\mu \rangle^2 , & P_5 &= -\frac{1}{2} \langle f_-^{\mu\nu} f_{-\mu\nu} \rangle , \\ P_2 &= \frac{1}{4} \langle u_\mu u_\nu \rangle \langle u^\mu u^\nu \rangle , & P_6 &= \frac{i}{4} \langle f_+^{\mu\nu} [u_\mu, u_\nu] \rangle , \\ P_3 &= \frac{1}{16} \langle \chi_+ \rangle^2 , & P_7 &= -\frac{1}{16} \langle \chi_- \rangle^2 . \\ P_4 &= \frac{i}{4} \langle u_\mu \chi_-^\mu \rangle , \end{aligned} \quad (4.8)$$

The following notation was used:

$$\begin{aligned} u_\mu &= iu^\dagger D_\mu U u^\dagger = -iu D_\mu U^\dagger u = u_\mu^\dagger , \\ \chi_\pm &= u^\dagger \chi u^\dagger \pm u \chi^\dagger u , \\ \chi_-^\mu &= u^\dagger D^\mu \chi u^\dagger - u D^\mu \chi^\dagger u ; \\ f_\pm^{\mu\nu} &= u F_L^{\mu\nu} u^\dagger \pm u^\dagger F_R^{\mu\nu} u , \end{aligned} \quad (4.9)$$

with  $u^2 = U$ . The field strength tensors  $F_{L,R}^{\mu\nu}$  are related to the nonabelian external fields  $r_\mu = v_\mu + a_\mu$ ,  $l_\mu = v_\mu - a_\mu$  through

$$\begin{aligned} F_R^{\mu\nu} &= \partial_\mu r_\nu - \partial_\nu r_\mu - i[r_\mu, r_\nu], \\ F_L^{\mu\nu} &= \partial_\mu l_\nu - \partial_\nu l_\mu - i[l_\mu, l_\nu]. \end{aligned} \quad (4.10)$$

The anomaly term  $\mathcal{L}_{WZW}$  contributes to  $V_8^{\mu\nu}$  [21]; we therefore simply neglect these contributions. The ellipses in (4.7) denote polynomials in the external fields which are independent of the pion variable. These terms do not contribute to S–matrix elements.

The realization of  $G$  on the fields in Eq. (4.9) is given by

$$I \xrightarrow{G} h(\phi) I h^\dagger(\phi), \quad (4.11)$$

where the non–linear realization  $h(\phi)$  defines the action of  $G$  on a coset element  $u(\phi)$  via

$$u(\phi) \xrightarrow{G} g_R u(\phi) h^\dagger(\phi) = h(\phi) u(\phi) g_L^\dagger. \quad (4.12)$$

Since the one–loop graphs generated by  $\mathcal{L}_2$  may be ultraviolet divergent, the low–energy constants  $l_i$  have to absorb these divergences leading to an ultraviolet finite representation of any contribution at  $\mathcal{O}(p^4)$ . Using dimensional regularization, the low–energy constants are defined [2] as

$$\begin{aligned} l_i &= l_i^r + \gamma_i \lambda, \quad i = 1, \dots, 7, \\ \lambda &= \frac{\mu^{2\omega}}{16\pi^2} \left\{ \frac{1}{2\omega} - \frac{1}{2} (\ln 4\pi + \Gamma'(1) + 1) \right\}, \end{aligned} \quad (4.13)$$

where  $l_i^r$  are the coupling constants renormalized at the scale  $\mu$ . The  $\gamma_i$  are displayed in Ref. [2].

Terms at  $\mathcal{O}(p^6)$  generated by  $Z_6$  contain two–loop diagrams with vertices from  $\mathcal{L}_2$ , one–loop graphs with one vertex from  $\mathcal{L}_4$  and tree diagrams generated by  $\mathcal{L}_6$ . The lagrangian  $\mathcal{L}_6$  in the mesonic sector was recently constructed by Fearing and Scherer [22]. In the case of  $SU(3) \times SU(3)$ , they find 111 (32) independent terms in the even (odd) intrinsic parity sector. In the even parity sector relevant here, the new low–energy constants that enter at this order have the form

$$B_i = B_i^r + B_i^d \quad i = 1, \dots, 111, \quad (4.14)$$

where the  $B_i^d$  contain poles and double poles at  $d = 4$ .

The amplitude generated by tree diagrams involving one vertex from  $\mathcal{L}_6$  contributes only a polynomial to  $\gamma\gamma \rightarrow \pi^+\pi^-$ , which has the same structure as the divergent part in the two–loop amplitude. To illustrate this fact, we note that the monomials [22]

$$\begin{aligned} \delta\mathcal{L}_6 &= B_{30} \langle [G^{\alpha\beta}]_+ [D_\mu D^\mu G_{\alpha\beta}]_+ \rangle \\ &+ B_{31} \langle [G^{\alpha\beta}]_+ [D_\alpha D^\gamma G_{\beta\gamma}]_+ \rangle \\ &+ B_{50} \langle [\chi]_+ \rangle \langle [G^{\mu\nu}]_+ [G_{\mu\nu}]_+ \rangle \end{aligned} \quad (4.15)$$

generate the polynomials

$$\begin{aligned} \delta A_6^C &= \frac{2}{9F^4} [(4B_{30} + 9B_{31})s - (8B_{30} + 112B_{50})M^2], \\ \delta B_6^C &= \frac{9}{2F^4} B_{31}. \end{aligned} \quad (4.16)$$

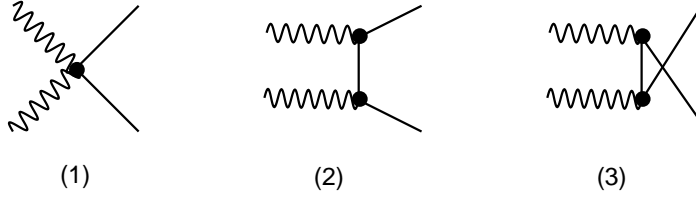


Figure 1: Tree diagrams contributing to  $Z_2$ . The mass in the propagators is identified with the physical pion mass at this order.

One may therefore remove the divergences in the two-loop amplitude by simply dropping the singular part. The finite pieces one is left with may be estimated via resonance exchange (see below). In the following, we use the notation

$$\begin{aligned}\delta A_6^C &= \frac{a_1^{r,c} M^2 + a_2^{r,c} s}{(16\pi^2 F^2)^2}, \\ \delta B_6^C &= \frac{b^{r,c}}{(16\pi^2 F^2)^2},\end{aligned}\tag{4.17}$$

for the total contribution from  $\mathcal{L}_6$ .

## 5 Results at $\mathcal{O}(p^2), \mathcal{O}(p^4)$

The process  $\gamma\gamma \rightarrow \pi^+\pi^-$  occurs already at tree level, in contrast to the situation in the neutral channel, where the leading term starts at one-loop order. The amplitude at tree level coincides with the one obtained from scalar electrodynamics,

$$\begin{aligned}A^C &= \left[ \frac{1}{M^2 - t} + \frac{1}{M^2 - u} \right] + \mathcal{O}(1), \\ B^C &= \frac{1}{2s} \left[ \frac{1}{M^2 - t} + \frac{1}{M^2 - u} \right] + \mathcal{O}(1).\end{aligned}\tag{5.1}$$

The pion mass in the propagators is identified with the physical one at this order in the expansion. The corresponding Feynman diagrams are depicted in Fig. 1. The next-to-leading term  $Z_4$  contains two types of contributions: one-loop graphs generated by  $\mathcal{L}_2$  and tree graphs involving one vertex from  $\mathcal{L}_4$ . The term proportional to the low-energy constant  $l_3$  in the lagrangian  $\mathcal{L}_4$  is quadratic in the fields. One may therefore shift the pion mass squared according to  $M^2 \rightarrow M_0^2 = M^2 + 2M^4 l_3 / F^2$  and from now on we denote the pion propagator by  $(M_0^2 - p^2)^{-1}$ , also in Fig. 1. Evaluating the several diagrams to  $\mathcal{O}(p^4)$  (Fig. 2) gives [6]

$$\begin{aligned}A^C &= \left[ \frac{1}{M_\pi^2 - t} + \frac{1}{M_\pi^2 - u} \right] + \frac{2}{F^2} \left[ \bar{G}(s) + \frac{\bar{l}_\Delta}{48\pi^2} \right] + \mathcal{O}(p^2), \\ B^C &= \frac{1}{2s} \left[ \frac{1}{M_\pi^2 - t} + \frac{1}{M_\pi^2 - u} \right] + \mathcal{O}(1).\end{aligned}\tag{5.2}$$



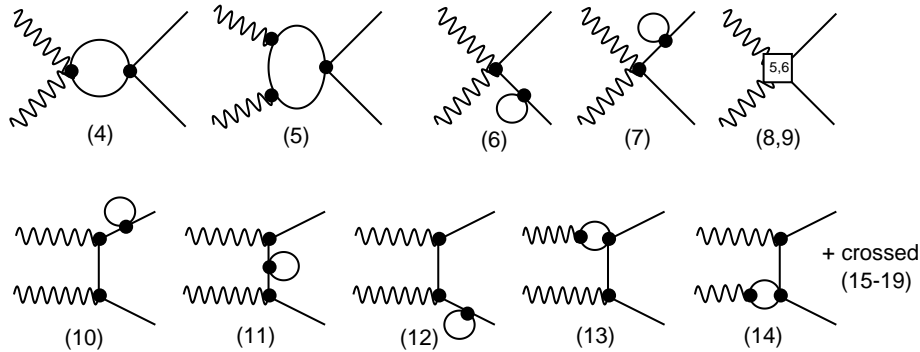


Figure 2: One-loop diagrams contributing to  $Z_4$ ; the graphs (4, 5) generate the finite loop function  $\bar{G}(s)$ . The graphs (10 –19) amounts to the replacement  $M^2 \rightarrow M_\pi^2$  in the tree result. Graphs (8, 9) stem from the lagrangian  $\mathcal{L}_4$ .

The loop function  $\bar{G}(s)$  is discussed in appendix A. The physical pion mass squared  $M_\pi^2$  is

$$M_\pi^2 = M^2 \left[ 1 + \frac{M^2}{F^2} \left( 2l_3^r + \frac{1}{32\pi^2} \ln \frac{M^2}{\mu^2} \right) + \mathcal{O}(M^4) \right]. \quad (5.3)$$

The pion decay constant  $F$  is identified at this order with the physical  $F_\pi$ . It is a specific feature of the process  $\gamma\gamma \rightarrow \pi^+\pi^-$  that, after mass renormalization, the one-loop contribution from  $\mathcal{L}_2$  is ultraviolet finite.  $\mathcal{L}_4$  generates the graphs (8,9) in Fig. 2. This contribution is proportional to the finite, scale independent combination

$$\bar{l}_\Delta = 96\pi^2(2l_5^r - l_6^r) = 2.7. \quad (5.4)$$

As is discussed in more detail in section 8.4, there is good agreement with the available experimental data and the chiral representation (5.2). We now turn to the evaluation of the contributions at order  $p^6$ .

## 6 Evaluation of diagrams at $\mathcal{O}(p^6)$

Up to  $\mathcal{O}(p^4)$  one has to deal with only a few Feynman diagrams for the process  $\gamma\gamma \rightarrow \pi^+\pi^-$  and the evaluation of the amplitude is straightforward. At  $\mathcal{O}(p^6)$  we have found remarkably many diagrams. To generate all graphs and to check the combinatorial factor for each of them, we use a beta-version of the *Mathematica* package *FeynArts 2.0* developed by S. Kueblbeck and H. Eck [23], where we have included the corresponding Feynman rules for CHPT, adapted to  $\gamma\gamma \rightarrow \pi^+\pi^-$ . In Fig. 3 we have plotted the full set of two-loop diagrams generated by  $\mathcal{L}_2$ . We have not distinguished the different intermediate pions running in the loops ( $\pi^1, \pi^2, \pi^3$ ). Each displayed diagram is the generating one for a class of subdiagrams with the same topology.

### 6.1 Two-loop diagrams from $\mathcal{L}_2$

The genuine two-loop diagrams 22 (vertex), 36,37 (box) and 45 (acnode) in Fig. 3 cannot be represented as products of one-loop integrals. A method to perform the relevant

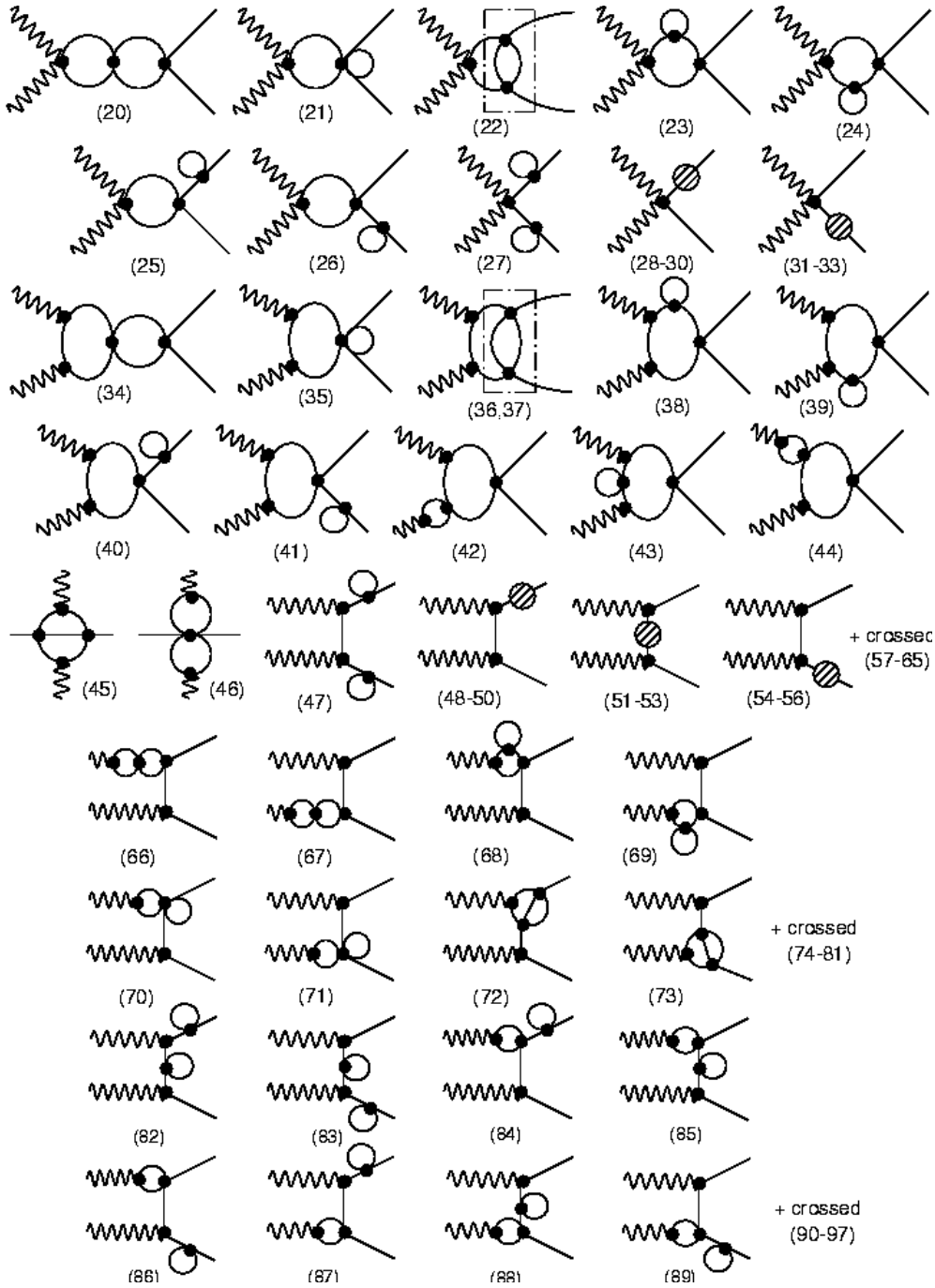


Figure 3: Full set of two-loop diagrams generated by  $\mathcal{L}_2$ . The vertex (22), box (36,37) and acnode (45) graphs are genuine two-loop diagrams, which do not have a representation in terms of one-loop functions. The dash-dotted boxes indicate subdiagrams which we have treated in the dispersive manner. We use symmetry arguments which relate the contributions from the reducible diagrams (47–97) to mass- and wavefunction corrections at two-loop order. The hatched circles summarize selfenergy contributions to the pion propagator (graphs (b – d) in Fig. 5).

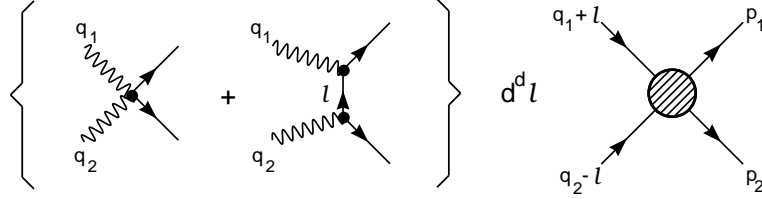


Figure 4: Construction scheme for a subclass of two-loop diagrams. The four-point function on the right-hand side is the  $d$ -dimensional elastic  $\pi\pi$ -amplitude at one-loop accuracy with two pions off-shell. The particles running between left and right are  $\pi^1$  and  $\pi^2$ . The symbol  $d^d l$  stands for integration over internal lines with weight (6.1).

momentum integrals is given in [9, 24, 25]. The graphs (20–26, 34–41) may be generated according to Fig. 4, where the four-point function on the right-hand side is the  $d$ -dimensional elastic  $\pi\pi$ -scattering amplitude at one-loop accuracy, with two pions off-shell. The loop integration over internal momenta with weight

$$\frac{1}{[M_\pi^2 - (l + q_1)^2] [M_\pi^2 - (q_2 - l)^2]}, \quad (6.1)$$

is indicated by the symbol  $d^d l$  in the figure.  $M_\pi^2$  denotes the physical pion mass in one-loop approximation (Eq. 5.3) and the momenta of the pions running in the loop are  $(l + q_1)^\mu$  and  $(q_2 - l)^\mu$ . This procedure has the advantage that the nonlocal singularities generated by divergent subdiagrams (enclosed by dash-dotted lines in the graphs (22,36,37)) are automatically removed [9].

A further comment concerns diagram (23) and (24). The tadpole in the loop propagator amounts to the replacement  $M^2 \rightarrow M_\pi^2$  if one also adds the one-loop diagram (4) in Fig. 2 multiplied with the wave function renormalization constant  $Z_\pi$  given at one-loop accuracy. A similar argument holds in the case of diagrams (38,39,42–44). Summing up these diagrams allows one to introduce the physical mass in the loop propagators.

The graphs (27–33) may be generated by multiplying the seagull diagram (Fig. 1, graph 3) with that part of the wave function renormalization constant  $Z_\pi$ , which is generated by  $\mathcal{L}_2$ . Furthermore, we use isospin symmetry arguments to handle the diagrams (47–97) that also incorporate the pion propagator at two-loop accuracy [24].

## 6.2 Pion propagator at $\mathcal{O}(p^6)$

We compute the correlator

$$\delta^{ab} \frac{1}{i} \Delta'_c(p^2) = \int d^D x e^{ipx} \langle 0 | T \phi^a(x) \phi^b(0) | 0 \rangle \quad (6.2)$$

in the  $\sigma$ -model parametrization Eq. (4.2). The complete propagator can be written in terms of the bare propagator  $\Delta'(p^2) = \frac{1}{i} \frac{1}{M^2 - p^2 - i\epsilon}$  and the self energy function  $\Sigma(p^2)$  in the standard manner,

$$\frac{1}{i} \Delta'_c(p^2) = \frac{1}{i} \frac{1}{M^2 - p^2 - i\epsilon} + \frac{1}{i} \frac{1}{M^2 - p^2 - i\epsilon} i\Sigma(p^2) \frac{1}{i} \frac{1}{M^2 - p^2 - i\epsilon} + \dots$$

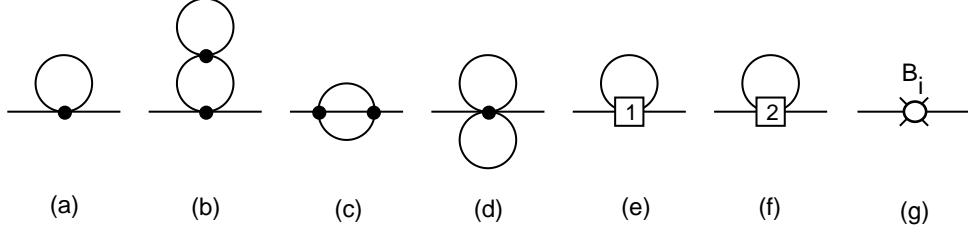


Figure 5: Selfenergy– graphs up to  $\mathcal{O}(p^6)$ . The contributions from diagram (a) start at  $\mathcal{O}(p^4)$ , whereas diagrams (b–g) are two–loop corrections. The sunset diagram (c) contributes to  $R(p^2)$ . The boxes in the graphs (e) and (f) denote vertices from the lagrangian  $\mathcal{L}_4$ , where the numbers indicate the corresponding low–energy constant. Diagram (g) contains the contribution from the lagrangian  $\mathcal{L}_6$  only.

$$\begin{aligned}
&= \frac{1}{i} \frac{1}{M^2 - p^2 - i\epsilon - \Sigma(p^2)} \\
&= \frac{1}{i} \left[ \frac{Z_\pi}{M_\pi^2 - p^2 - i\epsilon} + R(p^2) \right] .
\end{aligned} \tag{6.3}$$

In the last step we have developed the selfenergy function  $\Sigma(p^2)$  in a Taylor series around the physical mass  $M_\pi^2$ ,

$$\begin{aligned}
\Sigma(p^2) &= \Sigma(M_\pi^2) - (M_\pi^2 - p^2)\bar{\Sigma}(M_\pi^2) + (M_\pi^2 - p^2)^2 \bar{\bar{\Sigma}}(p^2) , \\
\bar{\Sigma}(M_\pi^2) &= \frac{\partial}{\partial p^2} \Sigma(p^2) \Big|_{p^2=M_\pi^2} , \\
R(p^2) &= - \frac{\bar{\bar{\Sigma}}(p^2)}{(1 + \bar{\Sigma}) [1 + \bar{\Sigma} - (M_\pi^2 - p^2) \bar{\bar{\Sigma}}(p^2)]} ,
\end{aligned} \tag{6.4}$$

where  $Z_\pi = (1 + \bar{\Sigma}(M_\pi^2))^{-1}$  is the residuum of the propagator. The physical mass is defined as the position of the pole of the propagator and we therefore have the implicit equation

$$M^2 - \Sigma(M_\pi^2) = M_\pi^2 , \tag{6.5}$$

which defines the physical mass  $M_\pi$  order by order.

Evaluating diagram (a) in Fig. 5 with the mass  $M_0^2 = M^2 + 2M^4 l_3 / F^4$  in the propagator and solving Eq. (6.5) one obtains the physical pion mass up to  $\mathcal{O}(p^4)$  given in Eq. (5.3). The wave function renormalization constant  $Z_\pi$  and the finite part of the propagator  $R(s)$  become at this order

$$Z_\pi = 1 - \frac{1}{F^2} F_1(M^2) , \quad R(s) = 0 , \quad [ \mathcal{O}(p^4) ] \tag{6.6}$$

where  $F_1(M^2)$  is a one–loop function defined in Eq. (A.4). At  $\mathcal{O}(p^6)$  the graphs (b–g) in Fig. 5 contribute to  $\Sigma$ . The diagrams (b–d) stem from the lagrangian  $\mathcal{L}_2$  whereas (e) and (f) are contributions from  $\mathcal{L}_4$ . The lagrangian  $\mathcal{L}_6$  contributes via diagram (g). Only the sunset graph (c) is nontrivial. The overlapping loop momenta in one of the propagators make the algebraic part tedious. Nevertheless for  $s = M_\pi^2$  the result of the

sunset selfenergy contribution may be obtained analytically. We find for the pion mass up to  $\mathcal{O}(p^6)$

$$M_\pi^2 = M^2 \left\{ 1 + \frac{M^2}{F^2} \left( \frac{F_1(M^2)}{2M^2} + 2l_3 \right) + \frac{M^4}{F^4} \left[ F_2(M^2) \left( F_2(M^2)p_M + \sum_{i=1}^3 l_i p_M^i \right) + B_M \right] \right\} + \mathcal{O}(M^8). \quad (6.7)$$

$B_M$  collects the contributions from the  $\mathcal{L}_6$  lagrangian and the polynomial  $p_M^i$  read

$$\begin{aligned} p_M &= \frac{17}{8} - \frac{79}{12}\omega + \frac{421}{32}\omega^2 + \mathcal{O}(\omega^3), \\ p_M^1 &= 14 - 15\omega + \frac{31}{2}\omega^2 + \mathcal{O}(\omega^3), \\ p_M^2 &= 8 - 10\omega + 11\omega^2 + \mathcal{O}(\omega^3), \\ p_M^3 &= 3 - 4\omega + 4\omega^2 + \mathcal{O}(\omega^3). \end{aligned} \quad (6.8)$$

$F_1, F_2$  are one-loop functions defined in Eq. (A.4). For the wave function renormalization constant  $Z_\pi$  we get at  $\mathcal{O}(p^6)$

$$Z_\pi = 1 - \frac{F_1(M^2)}{F^2} + \frac{M^4}{F^4} \left\{ F_2(M^2) \left( F_2(M^2)p_Z + \sum_{i=1}^3 l_i p_Z^i \right) + B_Z \right\} + \mathcal{O}(M^6), \quad (6.9)$$

where  $B_Z$  collects the contributions from the  $\mathcal{L}_6$  lagrangian and where

$$\begin{aligned} p_Z &= 1 - \frac{29}{6}\omega + \frac{395}{32}\omega^2 + \mathcal{O}(\omega^3), \\ p_Z^1 &= 14 - 15\omega + \frac{31}{2}\omega^2 + \mathcal{O}(\omega^3), \\ p_Z^2 &= 8 - 10\omega + 11\omega^2 + \mathcal{O}(\omega^3), \\ p_Z^3 &= 2 + \mathcal{O}(\omega^3). \end{aligned} \quad (6.10)$$

Furthermore  $R(s)$  becomes

$$\begin{aligned} R(s) &= \frac{F_2^2(M^2)}{F^4} p_R + \frac{1}{6F^4} \frac{h_F(s)}{(s - M^2)^2}, \\ p_R &= -\frac{3}{4}M^2 + \left( \frac{5}{4}M^2 - \frac{1}{12}s \right) \omega - \left( \frac{53}{16}M^2 + \frac{5}{32}s \right) \omega^2 + \mathcal{O}(\omega^3), \end{aligned} \quad (6.11)$$

with

$$\begin{aligned} h_F(s) &= \int_{4M_\pi^2}^{\infty} d\sigma \beta(\sigma) \int_0^1 dx \{ 6sM^4 + (1 - 12x + 18x^2)s^2M^2 \} \mathcal{K}(x, s), \\ \mathcal{K}(x, s) &= -\frac{1}{(16\pi^2)^2} \left\{ \ln \frac{z_2(x, s)}{z_2(x, M^2)} + \frac{(s - M^2)x(1 - x)}{z_2(x, M^2)} \right\}, \\ z_2(x, s) &= [M^2 - s(1 - x)]x + \sigma(1 - x), \end{aligned} \quad (6.12)$$

and where  $\beta(\sigma) = \sqrt{1 - 4M^2/\sigma}$ . The loop function  $h_F$  stems from the sunset diagram (c) in Fig. 5.

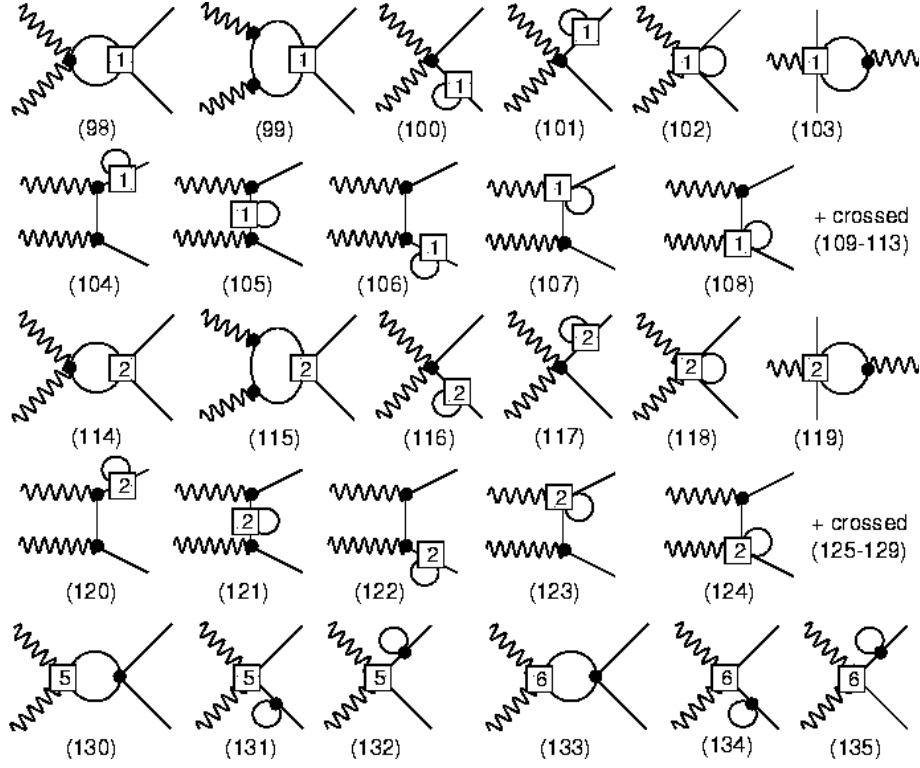


Figure 6: One-loop order contributions generated by the lagrangians  $\mathcal{L}_2 + \mathcal{L}_4$  with one vertex from  $\mathcal{L}_4$ . The boxes denote  $\mathcal{L}_4$ -couplings, whereas the numbers indicate the corresponding low-energy constant.

### 6.3 Contributions with one vertex from $\mathcal{L}_4$

We discuss some aspects of one-loop graphs generated by  $\mathcal{L}_2 + \mathcal{L}_4$  with one vertex from the lagrangian  $\mathcal{L}_4$  depicted in Fig. 6. Only diagrams proportional to  $(l_1, l_2, l_5, l_6)$  contribute to the process  $\gamma\gamma \rightarrow \pi^+\pi^-$ . The low energy constants  $l_3$  and  $l_4$  enter the two-loop amplitude through mass- and pion decay constant corrections. The diagrams (98,99) and (114,115) in Fig. 6 may be generated according to Fig. 4 where the  $\mathcal{L}_4$ -vertex is contained in the  $d$ -dimensional elastic  $\pi\pi$ -scattering amplitude at one-loop accuracy. These graphs remove the subdivergences indicated in Fig. 4 (enclosed by a dash-dotted line in graphs (22,36)).

The diagrams (100,101) and (116,117) may be included in the replacement  $Z_\pi \otimes$  seagull and the graphs (104–113), (120–129) are included in the replacement  $M^2 \rightarrow M_\pi^2$  in the reducible Born diagrams. The remaining graphs require straightforward one-loop calculation.

### 6.4 Counterterms with one vertex from $\mathcal{L}_6$

The diagrams depicted in Fig. 7 and generated by the lagrangian  $\mathcal{L}_6$  contribute a polynomial piece only. The divergent parts of the couplings cancel the pole structure generated by the two-loop diagrams. We have estimated the finite parts of these couplings by resonance exchange (see below).

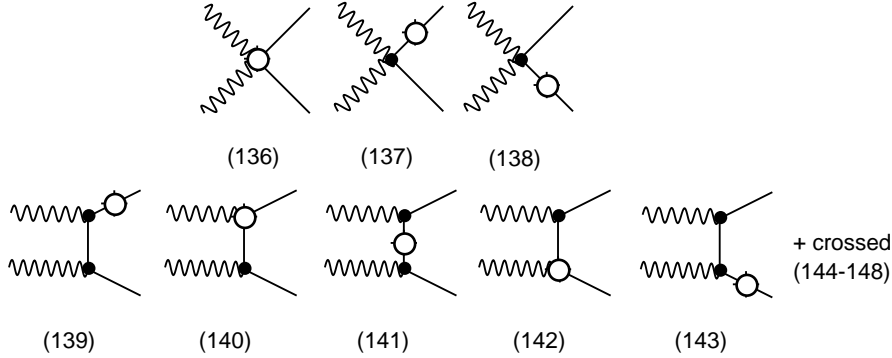


Figure 7: Tree order counterterms generated by  $\mathcal{L}_2 + \mathcal{L}_4 + \mathcal{L}_6$  with one vertex from  $\mathcal{L}_6$  denoted by a white circle. Diagrams (137–139,141,143) denote mass corrections in the propagators.

This concludes the discussion of the diagrams which occur at two-loop order in  $\gamma\gamma \rightarrow \pi^+\pi^-$ . For a complete mathematical treatment of all genuine graphs occurring in  $\gamma\gamma \rightarrow \pi^+\pi^-$  ( $\gamma\gamma \rightarrow \pi^0\pi^0$ ) see [24, 25].

## 7 Checks

The tensorial decomposition of the amplitude (2.4) leads to formfactors  $c_i(s, \nu)$  (see [9]), which are linearly related through two Ward identities and through Bose symmetry,

$$\begin{aligned}
 L_1(c_i) &\doteq 2c_0 + sc_4 - (t - u)c_5 = 0, \\
 L_2(c_i) &\doteq sc_7 - (t - u)c_9 = 0, \\
 L_3(c_i) &\doteq c_5 + c_7 = 0.
 \end{aligned} \tag{7.1}$$

The amplitudes  $A^C$  and  $B^C$  may be obtained from  $c_4$  and  $c_9$ ,

$$A = -c_4, \quad B = c_9/2s. \tag{7.2}$$

We have evaluated the five formfactors  $c_0, c_4, c_5, c_7$  and  $c_9$  in  $d$  dimensions and afterward the following consistency checks were made:

- (i) We have checked that the relations (7.1) below threshold are satisfied numerically within machine accuracy in low dimensions.
- (ii) By letting  $\omega \rightarrow 0$  and omitting the tree contributions generated by  $\mathcal{L}_2 + \mathcal{L}_4 + \mathcal{L}_6$  in Fig. 7, the formfactors  $c_i$  at order  $p^6$  have the structure

$$\begin{aligned}
 c_i(s, \nu) &= \frac{F_2(M^2)}{F^4} \left\{ F_2(M^2) [a_0^i + a_1^i \omega + a_2^i \omega^2 + \mathcal{O}(\omega^3)] \right. \\
 &\quad \left. + \sum_{j=1,2,5,6} l_j [b_0^{ij} + b_1^{ij} \omega + b_2^{ij} \omega^2 + \mathcal{O}(\omega^3)] \right\} \\
 &= \mu^{4\omega} \left\{ \frac{P_i^{(2)}}{4\omega^2} + \frac{P_i^{(1)}}{2\omega} + R_i + \mathcal{O}(\omega) \right\}.
 \end{aligned} \tag{7.3}$$

Table 1: Coefficients of the amplitude expansion in Eq. (7.3)

|            | $i = 0$  | $i = 4$                                  | $i = 5$              | $i = 7$             | $i = 9$           |
|------------|--|--|----------------------|---------------------|-------------------|
| $a_0^i$    | $-\frac{2}{9}M^2s + \frac{1}{18}s^2 - \frac{1}{18}\nu^2$         | $\frac{4}{9}M^2 - \frac{1}{9}s$          | $-\frac{1}{9}\nu$    | $\frac{1}{9}\nu$    | $\frac{1}{9}s$    |
| $a_1^i$    | $\frac{337}{216}M^2s - \frac{127}{864}s^2 - \frac{53}{864}\nu^2$ | $-\frac{337}{108}M^2 + \frac{127}{432}s$ | $-\frac{53}{432}\nu$ | $\frac{53}{432}\nu$ | $\frac{53}{432}s$ |
| $b_0^{i1}$ | $\frac{10}{3}M^2s + \frac{1}{6}s^2 - \frac{1}{6}\nu^2$           | $-\frac{20}{3}M^2 - \frac{1}{3}s$        | $-\frac{1}{3}\nu$    | $\frac{1}{3}\nu$    | $\frac{1}{3}s$    |
| $b_1^{i1}$ | $-4M^2s$   | $8M^2$                                   | 0                    | 0                   | 0                 |
| $b_0^{i2}$ | $-3M^2s + \frac{1}{4}s^2 - \frac{1}{4}\nu^2$                     | $6M^2 - \frac{1}{2}s$                    | $-\frac{1}{2}\nu$    | $\frac{1}{2}\nu$    | $\frac{1}{2}s$    |
| $b_1^{i2}$ | $2M^2s$  | $-4M^2$                                  | 0                    | 0                   | 0                 |
| $b_0^{i5}$ | $8M^2s + 2s^2$   | $-16M^2 - 4s$                            | 0                    | 0                   | 0                 |
| $b_1^{i5}$ | $-8M^2s$   | $16M^2$                                  | 0                    | 0                   | 0                 |
| $b_0^{i6}$ | $-4M^2s - s^2$   | $8M^2 + 2s$                              | 0                    | 0                   | 0                 |
| $b_1^{i6}$ | $4M^2s$  | $-8M^2$                                  | 0                    | 0                   | 0                 |

where  $a_k^i$  and  $b_k^{ij}$ ,  $k = 0, 1$  are polynomials in the external momenta and the pion mass (Table 1) and  $F_2(M^2)$  is a loop function defined in Eq. (A.4). The coefficients  $a_2^i$  and  $b_2^{ij}$  contain a polynomial part as well as complicated analytic functions and contribute to the finite part  $R_i$  of the amplitude.

We have verified that the residues  $P_i^{(k)}$  are polynomials in the external momenta and the pion mass. These polynomials obey Eq. (7.1) as well,

$$L_m(P_i^{(k)}) = 0, \quad m = 1, 2, 3, \quad k = 1, 2. \quad (7.4)$$

We have checked numerically that

$$L_m(R_i) = 0, \quad m = 1, 2, 3, \quad (7.5)$$

within machine accuracy below threshold. To go to the physical region for pion-pair production we have written fixed- $t$  dispersion relations for the box- and vertex parts. Matching the dispersive analysis with the non-dispersive expressions below threshold ensures that  $L_m(R_i) = 0$  is also satisfied above threshold.

- (iii) We have worked out the S-wave projection  $h_{C,+}^0(s)$  (2.9) for the helicity amplitude  $H_{++}^C$  and we have verified numerically that these amplitudes admit the correct phase at  $s > 4M_\pi^2$ , given by the (tree+one-loop) elastic  $\pi\pi$  scattering S-wave phase shifts (in the appropriate isospin decomposition).

## 8 Amplitude and cross section to two loops



## 8.1 Analytic results of the amplitude

We find for the two-loop amplitude  $A^C$

$$A^C = A_2^C + A_4^C + A_6^C + \mathcal{O}(p^4), \quad (8.1)$$

or

$$A^C = \left\{ \frac{1}{M_\pi^2 - t} + \frac{1}{M_\pi^2 - u} \right\} + \frac{2}{F_\pi^2} \left\{ \bar{G}_\pi(s) + \frac{\bar{l}_\Delta}{48\pi^2} \right\} + U_A^C + P_A^C + \mathcal{O}(p^4). \quad (8.2)$$

The unitary part  $U_A^C$  contains  $s$ ,  $t$  and  $u$ - channel cuts, and  $P_A^C$  is a linear polynomial in  $s$ . Explicitly we find,

$$\begin{aligned} U_A^C &= \frac{1}{sF_\pi^4} \bar{G}(s) [ (2M_\pi^4 - 4M_\pi^2 s + 3s^2) \bar{J}(s) + C^C(s, \bar{l}_i) ] + \frac{\bar{l}_\Delta}{48\pi^2 F_\pi^4} s \bar{J}(s) \\ &+ \frac{(\bar{l}_1 - \frac{4}{3})}{288\pi^2 s F_\pi^4} (s - 4M_\pi^2) \{ \bar{H}(s) + 4 [ s \bar{G}(s) + 2M_\pi^2 (\bar{G}(s) - 3 \bar{J}(s)) ] d_{00}^2 \} \\ &+ \frac{(\bar{l}_2 - \frac{5}{6})}{96\pi^2 s F_\pi^4} (s - 4M_\pi^2) \{ \bar{H}(s) + 4 [ s \bar{G}(s) + 2M_\pi^2 (\bar{G}(s) - 3 \bar{J}(s)) ] d_{00}^2 \} \\ &+ \Delta_A^C(s, t, u), \end{aligned} \quad (8.3)$$

with

$$\begin{aligned} C^C(s, \bar{l}_i) &= \frac{1}{48\pi^2} \left\{ \frac{1}{3} (\bar{l}_1 - \frac{4}{3}) (16s^2 - 56M_\pi^2 s + 64M_\pi^4) + (\bar{l}_2 - \frac{5}{6}) (8s^2 - 24M_\pi^2 s + 32M_\pi^4) \right. \\ &\quad \left. - 12M_\pi^4 \bar{l}_3 + 12M_\pi^2 s \bar{l}_4 - 12M_\pi^2 s + 12M_\pi^4 \right\}, \\ d_{00}^2 &= \frac{1}{2} (3 \cos^2 \theta - 1). \end{aligned} \quad (8.4)$$

The loop functions  $\bar{J}$  etc. are displayed in appendix A and  $\bar{G}_\pi(s)$  in Eq. (8.2) stands for  $\bar{G}(s)$  evaluated with the physical mass. The term proportional to  $d_{00}^2$  in  $U_A^C$  contributes to  $D$ -waves only. For  $\Delta_A^C$  see below. The polynomial part is

$$\begin{aligned} P_A^C &= \frac{1}{(16\pi^2 F_\pi^2)^2} [ a_1^c M_\pi^2 + a_2^c s ], \\ a_1^c &= a_1^{c,r} + \frac{1}{9} \{ 4l^2 + l(-10\bar{l}_1 + 18\bar{l}_2 - 12\bar{l}_\Delta + \frac{337}{6}) - \frac{5}{3}\bar{l}_1 - 5\bar{l}_2 + 12\bar{l}_4 \bar{l}_\Delta + 4 \}, \\ a_2^c &= a_2^{c,r} - \frac{1}{9} \{ l^2 + l(\frac{1}{2}\bar{l}_1 + \frac{3}{2}\bar{l}_2 + 3\bar{l}_\Delta + \frac{127}{24}) - \frac{5}{12}\bar{l}_1 - \frac{5}{4}\bar{l}_2 + 3\bar{l}_\Delta + \frac{21}{2} \}, \\ l &= \ln \frac{M_\pi^2}{\mu^2}. \end{aligned} \quad (8.5)$$

The result for  $B^C$  reads

$$B^C = B_2^C + B_6^C + \mathcal{O}(p^2), \quad (8.6)$$

or

$$B^C = \frac{1}{2s} \left\{ \frac{1}{M_\pi^2 - t} + \frac{1}{M_\pi^2 - u} \right\} + U_B^C + P_B^C + \mathcal{O}(p^2), \quad (8.7)$$

with the unitary part

$$U_B^C = \frac{1}{192\pi^2 s F_\pi^4} \left\{ \frac{1}{3} (\bar{l}_1 - \frac{4}{3}) + (\bar{l}_2 - \frac{5}{6}) \right\} \bar{H}(s) + \Delta_B^C(s, t, u). \quad (8.8)$$

For the polynomial part we find

$$\begin{aligned}
P_B^C &= \frac{b^c}{(16\pi^2 F_\pi^2)^2}, \\
b^c &= b^{c,r} - \frac{1}{18} \left\{ l^2 + l \left( \frac{1}{2} \bar{l}_1 + \frac{3}{2} \bar{l}_2 - \frac{53}{24} \right) - \frac{1}{12} \bar{l}_1 - \frac{1}{4} \bar{l}_2 + \frac{7}{2} \right\}. \quad (8.9)
\end{aligned}$$

The integrals  $\Delta_{A,B}^C(s, t, u)$  contain contributions from the two-loop box-, vertex- and acnode graphs and also from the reducible diagrams manifest in the function  $R(s)$  given in Eq. (6.11). We discuss the size of these corrections in section 8.3.

## 8.2 Low-energy constants

The Born contribution to the charged pion-pair production contains  $M_\pi$  as the only parameter. At next-to-leading order three parameters occur, namely,  $M_\pi, F_\pi, \bar{l}_6 - \bar{l}_5$ . Going to the two-loop correction the number of parameters increases. Once the program described in section 6 is carried through, the ultraviolet finite and scale independent amplitudes  $A^C$  and  $B^C$  contain the set  $M_\pi, F; l_i^r, l_{i1}^r$  ( $i = 1, 2, 3, 5, 6$ );  $a_1^{r,c}, a_2^{r,c}$  and  $b^{r,c}$  low-energy constants. The couplings  $l_{i1}^r$  stem from the  $\mathcal{O}(\omega)$ -part in the expansion of the  $\mathcal{L}_4$  low-energy parameters, whereas  $a_1^{r,c}, a_2^{r,c}$  and  $b^{r,c}$  are couplings from the lagrangian  $\mathcal{L}_6$ .  $F$  is related to the pion decay constant  $F_\pi$  [2]

$$F_\pi = F \left[ 1 + \frac{M^2}{F^2} \left( l_4^r - \frac{1}{16\pi^2} \ln \frac{M^2}{\mu^2} \right) + \mathcal{O}(M^4) \right]. \quad (8.10)$$

We may therefore replace  $F$  by  $F_\pi$  at the expense of introducing  $l_4^r$ . The expressions for the loop-amplitudes simplify if one uses the scale-independent parameters  $\bar{l}_i$  instead of  $l_i^r$ ,

$$l_i^r = \frac{\gamma_i}{32\pi^2} (\bar{l}_i + \ln \frac{M^2}{\mu^2}). \quad (8.11)$$

The values of the  $\bar{l}_i$  are depicted in Table 2 together with the experimental sources and the values for the  $\gamma_i$ . The couplings  $l_{i1}^r$  contribute a polynomial piece only and may therefore be absorbed into the low-energy constants at order  $p^6$  [27]. We are therefore left with  $a_1^{r,c}, a_2^{r,c}$  and  $b^{r,c}$  as the only new unknowns. The coupling constants occurring at  $\mathcal{O}(p^4)$  in the low-energy expansion are dominated by the low-lying vector, axial-vector, scalar and pseudoscalar resonances in such a way, that they practically saturate the corresponding couplings of the  $\mathcal{O}(p^4)$  effective lagrangian [2, 28].

Here we assume that this is also true at order  $p^6$ . We estimate the renormalized couplings  $a_1^{r,c}, a_2^{r,c}$  and  $b^{r,c}$  by replacing them at a scale  $\mu = 500 \text{ MeV} \dots 1 \text{ GeV}$  by the contribution from resonance exchange. Let

$$I^{c,r}(\mu) = \sum_{R=\rho, a_1, b_1} I^R + \hat{I}^r(\mu), \quad I = a_1, a_2, b, \quad (8.12)$$

where the sum denotes contributions from vector- ( $J^{PC} = 1^{--}$ ) and axial-vector ( $J^{PC} = 1^{++}, 1^{+-}$ ) exchange [11, 29–32] with meson mass  $M_R \leq 1.2 \text{ GeV}$ . The non-resonance contribution of these low-energy constants has to be chosen in such a way that the final result of the amplitudes  $A^C$  and  $B^C$  is scale independent. Our estimate for  $I^{c,r}(M_\rho)$  consists in setting  $\hat{I}^r(M_\rho) = 0$ .

Table 2: Low-energy constants and sources. In the fourth column we have plotted the  $\gamma_i$  evaluated in [2, 26]

| i | $\bar{l}_i$    | Source                              | $\gamma_i$ |
|---|----------------|-------------------------------------|------------|
| 1 | $-1.7 \pm 1.0$ | $K_{e4}, \pi\pi \rightarrow \pi\pi$ | 1/3        |
| 2 | $6.1 \pm 0.5$  | $K_{e4}, \pi\pi \rightarrow \pi\pi$ | 2/3        |
| 3 | $2.9 \pm 2.4$  | $SU(3)$ mass formulae               | -1/2       |
| 4 | $4.3 \pm 0.9$  | $F_K/F_\pi$                         | 2          |
| 5 | $13.8 \pm 1.3$ | $\pi \rightarrow e\nu\gamma$        | -1/6       |
| 6 | $16.5 \pm 1.1$ | $\langle r^2 \rangle_V^\pi$         | -1/3       |

Table 3: Resonance contributions to the constants  $a_1^{r,c}, a_2^{r,c}$  and  $b^{r,c}$ . The calculation is done in [24], the uncertainties are more generous than quoted in that reference.

| $I^r$       | $I^R$  |       |       | $\sum_R I^R$    |
|-------------|--------|-------|-------|-----------------|
|             | $\rho$ | $a_1$ | $b_1$ |                 |
| $a_1^{r,c}$ | -3.28  | 0     | 0     | $-3.3 \pm 1.65$ |
| $a_2^{r,c}$ | 1.23   | -0.35 | -0.13 | $0.75 \pm 0.65$ |
| $b^{r,c}$   | 0.20   | 0.18  | 0.06  | $0.45 \pm 0.15$ |

The quantities  $I^R$  are evaluated in [24]. The results of this calculation are displayed in Table 3 where the individual resonance contributions  $I^R$  are listed. Column 5 contains the sums of the several contributions provided with a systematic error. We associate a 50% uncertainty to the contributions generated by (axial-) vector exchange.

It is useful to consider furthermore the helicity amplitudes  $H_{++}^C$  and  $H_{+-}^C$  and the corresponding low-energy constants  $h_{\pm}^{r,c}$  and  $h_s^{r,c}$ ,

$$\begin{aligned}
H_{++}^{C,2loops} &= \frac{h_+^{r,c} M^2 + h_s^{r,c} s}{(16\pi^2 F^2)^2} + \dots, \\
H_{+-}^{C,2loops} &= \frac{8(M^4 - tu)}{s(16\pi^2 F^2)^2} h_-^{r,c} + \dots, \\
h_+^{r,c} &= a_1^{r,c} + 8b^{r,c}, \quad h_s^{r,c} = a_2^{r,c} - 2b^{r,c}, \quad h_-^{r,c} = b^{r,c}.
\end{aligned} \tag{8.13}$$

Adding the errors quoted in Table 3 in quadrature, we find

$$\begin{aligned}
h_+^{r,c}(M_\rho) &= 0.3 \pm 2.0, \\
h_s^{r,c}(M_\rho) &= -0.15 \pm 0.7, \\
h_-^{r,c}(M_\rho) &= 0.45 \pm 0.15.
\end{aligned} \tag{8.14}$$

This completes the determination of the parameters which occur at two-loop order in  $\gamma\gamma \rightarrow \pi^+\pi^-$ .

### 8.3 Numeric results of the amplitude

The characteristics of the two-loop corrections may be seen in Fig. 8, where we have plotted the real and imaginary part of the helicity amplitudes  $10^{-3}M_\pi^2\bar{H}_{+\pm}^C$  (2.10) at  $t = u$ . All curves start at  $E = 280$  MeV and the crosses refer to the center-of-mass energy of the  $\pi^+\pi^-$  system in 100 MeV steps<sup>3</sup>. The solid line incorporates all contributions stemming from the one- and two-loop calculation only. The dash-dotted line is the same amplitude without  $\Delta_{A,B}^C$ . The dotted line corresponds to the one-loop result (apart from mass renormalization terms,  $\bar{H}_{+-}^C$  does not receive any contribution from one-loop diagrams). To get some feeling about the size of the genuine two-loop diagrams, we have drawn with a dashed line the contributions from the sum of one-loop and acnode graphs, with a dashed-double dotted line the sum of the one-loop and box diagrams at the scale  $\mu = 770$  MeV in the  $\overline{MS}$  chiral scheme.

### 8.4 Cross section $\gamma\gamma \rightarrow \pi^+\pi^-$

The cross section for  $\gamma\gamma \rightarrow \pi^+\pi^-$  in the framework of  $SU(3) \times SU(3)$  CHPT was worked out up to  $\mathcal{O}(p^4)$  in [6]. The amplitude at this order contains only the three low-energy parameters  $F_\pi, M_\pi$  and  $\bar{l}_\Delta$ . We note that the increase in the cross section around the peak at  $\sqrt{s} = 306$  MeV due to the one-loop correction is  $\sim 15\%$  where the renormalization scale independent counterterm contribution  $\sim \bar{l}_\Delta$  amounts  $\sim 50\%$  of this correction. Furthermore it is instructive to compare the cross section with the one from  $\gamma\gamma \rightarrow \pi^0\pi^0$  scattering [9]. In the neutral case the size of the cross section is two orders of magnitude smaller than in the charged channel, since the neutral amplitude starts out with one-loop diagrams, whereas in the charged case the Born amplitude contributes dominantly to the cross section: At low energies the photon couples to the charge of the pions. As a result of this, the  $\gamma\gamma \rightarrow \pi^0\pi^0$  cross section is small, while that for  $\gamma\gamma \rightarrow \pi^+\pi^-$  is large.

The plot in Fig. 9 shows the total cross section  $\sigma(s; |\cos\theta| \leq Z = 0.6)$  as a function of the center-of-mass energy  $E = \sqrt{s}$ . Here we choose  $Z = 0.6$  to compare with the available data from the Mark II collaboration [10]. The Born contribution is displayed with a dotted line whereas the born+one-loop cross section is shown with a dashed line. Also at this order the chiral expansion is in remarkable agreement with the available data. The solid line incorporates all contribution up to  $\mathcal{O}(p^6)$ . It is seen that the two-loop effect changes the one-loop result only very little. Switching off the integrals  $\Delta_{A,B}^C$  does not affect the cross section visibly. This fact is also clear by consulting Fig. 8, from where it is seen that our explicit, compact representation of the two-loop amplitudes is rather accurate. We note that the two-loop correction, mainly dominated by the effect of final state  $\pi\pi$  interaction, enhances the cross section very close to threshold and then suppress it above  $E = 350$  MeV, see Fig. 9. Finally, the dashed-double dotted line displays the result of a dispersive analysis (Fig. 7 in Ref. [11]). In that calculation, use was made of a doubly subtracted dispersion relation with the subtraction constants determined in terms of chiral counterterms, incorporating also heavy meson exchange.

<sup>3</sup>We use  $F_\pi = 92.4$  MeV,  $M_\pi = 139.6$  MeV and  $\bar{l}_1 = -1.7 \pm 1.0$ ,  $\bar{l}_2 = 6.1 \pm 0.5$ ,  $\bar{l}_3 = 2.9 \pm 2.4$ ,  $\bar{l}_4 = 4.3 \pm 0.9$ ,  $\bar{l}_\Delta = 2.7 \pm 0.4$  throughout.

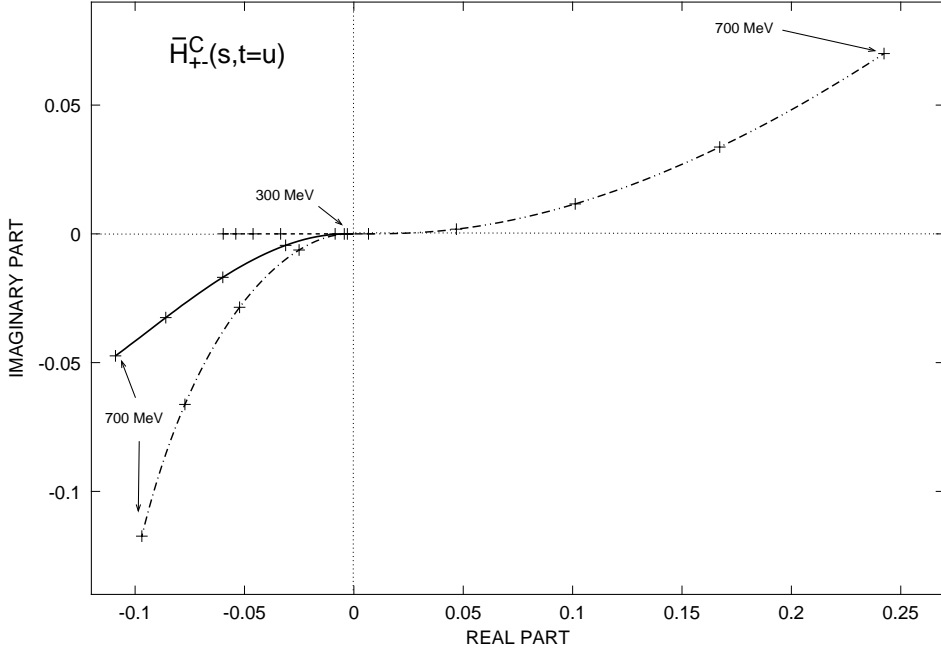
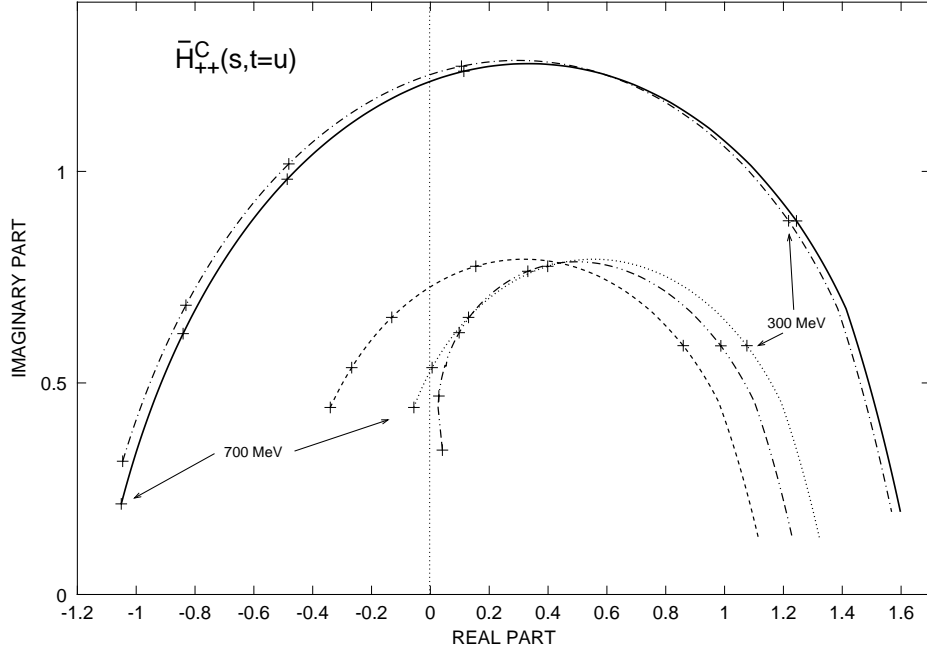


Figure 8: Real and imaginary part of the helicity amplitude  $10^{-3}M_\pi^2\bar{H}_{\pm\pm}^C$  at  $t = u$ . The solid line incorporates all contributions from one- and two-loop corrections. The dash-dotted line is the same amplitude with the omission of  $\Delta_{A,B}^C$ . The dotted line corresponds to the one-loop result (apart from mass renormalization terms,  $\bar{H}_{+-}^C$  does not receive any contribution from one-loop diagrams – the dotted line is therefore absent in the lower figure). The dashed line is the sum of the one-loop and acnode, the dashed-double dotted the sum of the one-loop and box contribution at the scale  $\mu = 770$  MeV in the  $\overline{MS}$  chiral scheme. Finally the crosses refer to the center-of-mass energy of the  $\pi^+\pi^-$  system in 100 MeV steps.

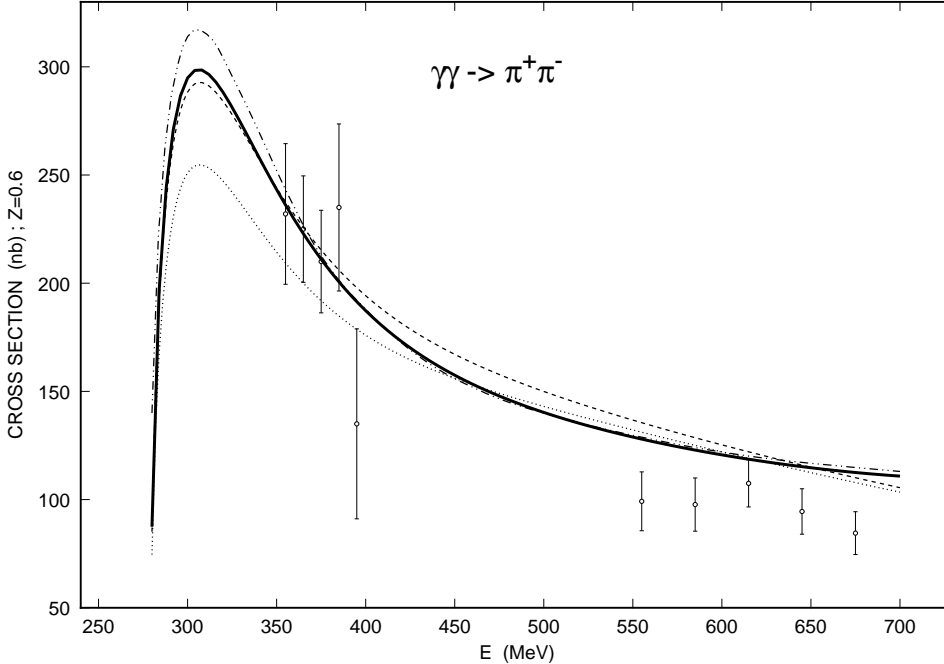


Figure 9: The  $\gamma\gamma \rightarrow \pi^+\pi^-$  cross section  $\sigma(s; |\cos\theta| \leq Z = 0.6)$  as a function of the center-of-mass energy  $E$ , together with the data from the Mark II collaboration [10]. We have added in quadrature the tabulated statistical and systematical errors. In addition, there is an overall normalization uncertainty of 7% in the data [10]. The solid line is the full two-loop result, the dashed line corresponds to the one-loop approximation [6] and the dotted line is the Born contribution. The dashed-double dotted line is the result of a dispersive calculation performed by Donoghue and Holstein (Fig. 7 in Ref. [11]).

The two-loop result thus agrees very well with the data and shows furthermore a very good agreement for  $\sqrt{s} \geq 350$  MeV with the dispersive analysis of Donoghue and Holstein.

In Fig. 10 the effect of the low-energy constants is shown. The solid line corresponds to the two-loop result evaluated at  $\Delta_{A,B}^C = 0$  and without resonance exchange. (It turns out that the contributions from the resonances to the cross section are negligible below 450 MeV.) The dashed line corresponds to  $\bar{l}_i = 0$ , and the dash-dotted line is obtained by setting  $\bar{l}_1 = \bar{l}_3 = 0$ . Therefore the increase in the cross section is due to  $\bar{l}_2, \bar{l}_4$  and  $\bar{l}_\Delta$ , as was also shown in the neutral case [9].

## 9 Compton scattering and pion polarizability

Compton scattering on pions  $\gamma\pi^+ \rightarrow \gamma\pi^+$  is related to pion-pair production by crossing  $(p_1, q_1)^\mu \rightarrow -(p_1, q_1)^\mu, s \leftrightarrow t$ . The corresponding scattering amplitudes may again be expressed in terms of the amplitudes  $A^C$  and  $B^C$  as functions of the Mandelstam variables in the Compton channel,

$$\bar{s} = (q_1 + p_1)^2, \bar{t} = (q_2 - q_1)^2, \bar{u} = (p_2 - q_1)^2. \quad (9.1)$$

In the present section we discuss shortly the Compton cross section. Afterwards we work out the chiral expansion of the charged pion polarizabilities at next-to-leading order.

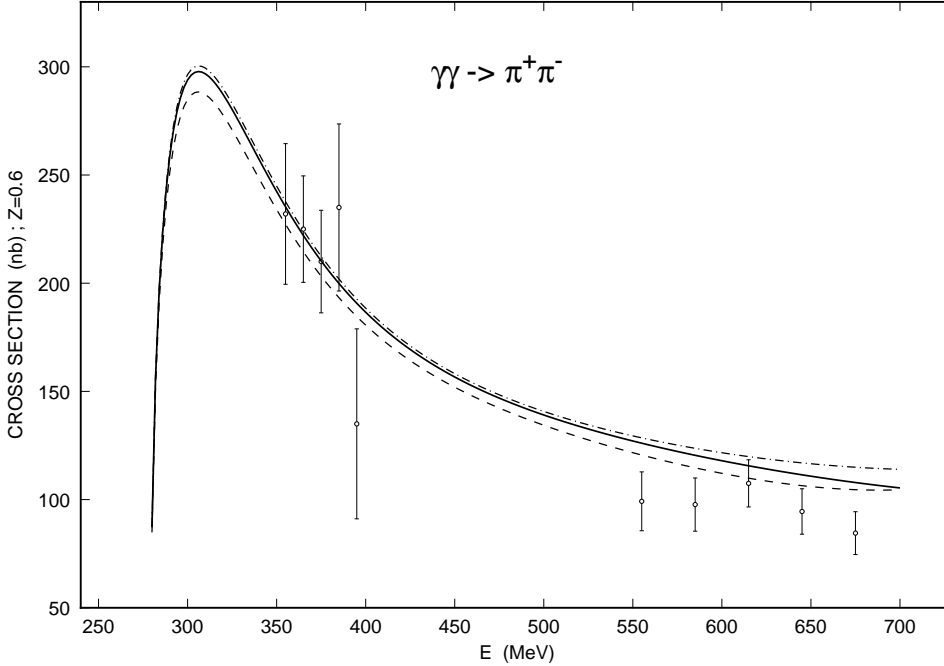


Figure 10: The  $\gamma\gamma \rightarrow \pi^+\pi^-$  cross section  $\sigma(s; |\cos\theta| \leq Z = 0.6)$  as a function of the center-of-mass energy  $E$ . The solid line is the two-loop result evaluated at  $\Delta_{A,B}^C = 0$  and without resonance exchange. The dashed line corresponds to  $\bar{l}_i = 0$ , whereas the dash-dotted line is obtained by setting  $\bar{l}_1 = \bar{l}_3 = 0$ .

### 9.1 Compton cross section $\gamma\pi^+ \rightarrow \gamma\pi^+$

The total cross section at tree level is given by [33]

$$\sigma^{\gamma\pi^+ \rightarrow \gamma\pi^+}(\bar{s}) = 4\alpha^2\pi \frac{M_\pi^2 + \bar{s}}{\bar{s}(M_\pi^2 - \bar{s})^3} \left[ M_\pi^4 - \bar{s}^2 + 2M_\pi^2 \bar{s} \ln \frac{\bar{s}}{M_\pi^2} \right]. \quad (9.2)$$

This quantity is plotted in Fig. 11 as a function of the center-of-mass energy  $E_{\gamma\pi}$ . At threshold one obtains the total Thomson cross section

$$\sigma^{\gamma\pi^+ \rightarrow \gamma\pi^+}(\bar{s} = M_\pi^2) = \frac{8\pi}{3} r_e^2, \quad (9.3)$$

where  $r_e = \alpha/M_\pi$  is the classical electromagnetic radius of the pion. Comparing the Compton cross section with the pion production case we note that the former is one order of magnitude bigger. The increase in the cross section due to one-loop corrections is smaller than one percent and the two-loop result is again smaller by a factor of 3. As a result of this, corrections in the charged Compton channel are negligible.

In the neutral channel, the leading term is generated by one-loop graphs. The cross section at  $E = 350$  MeV is three orders of magnitude smaller than in the charged case and tends to zero at threshold. Two-loop corrections are substantial, and the result for the Compton amplitude is therefore not very reliable at this order [9].

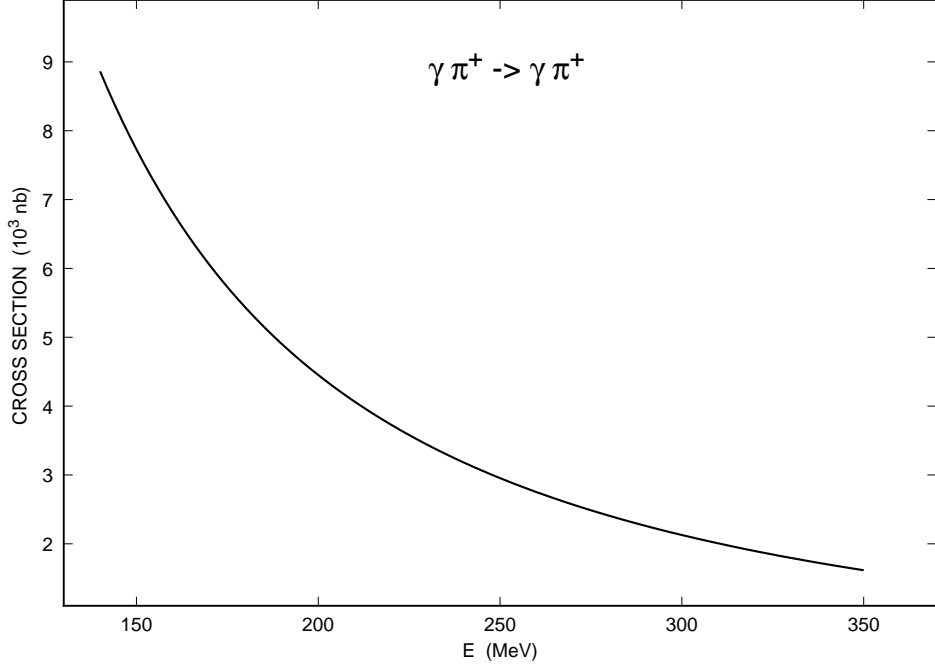


Figure 11: The Compton cross section as a function of the center-of-mass energy  $E = \sqrt{s}$  in Born approximation. One- and two-loop corrections are tiny in this case and would not be visible in the figure.

## 9.2 Chiral expansion of the pion polarizabilities

Among other fundamental parameters (mass, charge, magnetic moment, ...) the electromagnetic polarizabilities characterize a composite system like a hadron [34]. They parametrize the first correction in the Taylor series expansion of the Compton amplitude in photon energies at threshold,

$$T = -2 \left[ \vec{\epsilon}_1 \cdot \vec{\epsilon}_2^* (e^2 - 4\pi M_\pi \bar{\alpha}_\pi \omega_1 \omega_2) - 4\pi M_\pi \bar{\beta}_\pi (\vec{q}_1 \times \vec{\epsilon}_1) \cdot (\vec{q}_2 \times \vec{\epsilon}_2^*) + \dots \right], \quad (9.4)$$

with  $q_i^\mu = (\omega_i, \vec{q}_i)$ . In terms of the helicity amplitudes  $\bar{H}_{++}^C (J=0)$  and  $\bar{H}_{+-}^C (J=2)$  one has

$$\bar{\alpha}_{\pi^\pm} \pm \bar{\beta}_{\pi^\pm} = \frac{\alpha}{M_\pi} \lim_{s \rightarrow 0} \lim_{t \rightarrow M_\pi^2} \bar{H}_{+\mp}^C, \quad (9.5)$$

indicating that the combination  $\bar{\alpha}_{\pi^\pm} - \bar{\beta}_{\pi^\pm}$  is pure S-wave while  $\bar{\alpha}_{\pi^\pm} + \bar{\beta}_{\pi^\pm}$  is pure D-wave in the  $\gamma\pi^\pm \rightarrow \gamma\pi^\pm$  channel. Below we also use the notation

$$\begin{aligned} (\alpha \pm \beta)^C &= \bar{\alpha}_{\pi^\pm} \pm \bar{\beta}_{\pi^\pm}, \\ (\alpha \pm \beta)^N &= \bar{\alpha}_{\pi^0} \pm \bar{\beta}_{\pi^0}. \end{aligned} \quad (9.6)$$

From the Compton scattering amplitude at threshold Eq. (9.4) expressed through the functions  $A^C$  and  $B^C$  (see Eqs. (8.2, 8.7)) it is straightforward to determine the chiral expansion of the pion polarizabilities in terms of the quark masses to two loops,

$$(\alpha \pm \beta)^{N,C} = \frac{\alpha}{16\pi^2 M_\pi F_\pi^2} \left\{ A_\pm^{N,C} + \frac{M_\pi^2 B_\pm^{N,C}}{16\pi^2 F_\pi^2} + \mathcal{O}(M_\pi^4) \right\}. \quad (9.7)$$



The leading result is given in [16]

$$A_{\pm}^N = \begin{pmatrix} 0 \\ -\frac{1}{3} \end{pmatrix}, \quad A_{\pm}^C = \begin{pmatrix} 0 \\ \frac{2}{3}\bar{l}_{\Delta} \end{pmatrix}. \quad (9.8)$$

The next-to-leading order terms  $B_{\pm}^N$  have been determined in [9]. We find the following expressions for the coefficients  $B_{\pm}^C$

$$\begin{aligned} B_+^C &= 8h_-^{r,c}(\mu) - \frac{4}{9} \left\{ l(l + \frac{1}{2}\bar{l}_1 + \frac{3}{2}\bar{l}_2) - \frac{53}{24}l + \frac{1}{2}\bar{l}_1 + \frac{3}{2}\bar{l}_2 + \frac{91}{72} + \Delta_+^C \right\}, \\ B_-^C &= h_+^{r,c}(\mu) - \frac{4}{3} \left\{ l(\bar{l}_1 - \bar{l}_2 + \bar{l}_{\Delta} - \frac{65}{12}) - \frac{1}{3}\bar{l}_1 - \frac{1}{3}\bar{l}_2 + \frac{1}{4}\bar{l}_3 - \bar{l}_{\Delta}\bar{l}_4 + \frac{187}{108} + \Delta_-^C \right\}, \\ l &= \ln \frac{M_{\pi}^2}{\mu^2}, \end{aligned} \quad (9.9)$$

with

$$\begin{aligned} \Delta_+^C &= -18(16\pi^2 F_{\pi}^2)^2 \lim_{s \rightarrow 0} \lim_{t \rightarrow M_{\pi}^2} \Delta_B^C = -8.69, \\ \Delta_-^C &= -\frac{3}{4M_{\pi}^2}(16\pi^2 F_{\pi}^2)^2 \lim_{s \rightarrow 0} \lim_{t \rightarrow M_{\pi}^2} (\Delta_A^C + 8M_{\pi}^2 \Delta_B^C) = -8.73. \end{aligned} \quad (9.10)$$

Our final result of the charged pion polarizabilities including corrections up to  $\mathcal{O}(p^6)$  reads ( $\mu = M_{\rho}$ )

$$\begin{aligned} (\alpha + \beta)^C &= 0.3 \pm 0.1 && (0.0), \\ (\alpha - \beta)^C &= 4.4 \pm 1.0 && (5.4 \pm 0.8), \\ \bar{\alpha}_{\pi\pm} &= 2.4 \pm 0.5 && (2.7 \pm 0.4), \\ \bar{\beta}_{\pi\pm} &= -2.1 \pm 0.5 && (-2.7 \pm 0.4). \end{aligned} \quad (9.11)$$

The numbers in brackets denote the leading order result. The estimate of the errors only stems from the uncertainties in the couplings and do not contain effects from higher orders in the quark mass expansion or any correlations. (The errors are more generous than quoted in Ref. [24].) We use furthermore  $\bar{l}_{\Delta} = 2.7 \pm 0.4$  [2] extracted from the tree result ( $\mathcal{O}(p^4)$ ) of the radiative pion beta decay. Note however, that corrections in this process may change the error accordingly.

### 9.3 Data on pion polarizabilities

Performing Compton scattering on pions is not easy. Nevertheless, it is possible to probe the pion polarizability according to Fig. 12 by measuring the Compton scattering amplitude: (a) Pion photoproduction in photon-nucleus scattering  $\gamma p \rightarrow \gamma \pi^+ n$  [17], (b) Radiative pion nucleus scattering (Primakoff effect)  $\pi^- - Z \rightarrow \pi^- - \gamma Z$  [18] or (c,d) Pion-pair production in  $e^+e^-$  collisions. Analyzing the data with the constraint  $(\alpha + \beta)^C = 0$  gives

$$(\alpha - \beta)^C = \begin{cases} 40 \pm 24 & (\text{Lebedev [17]}), \\ 13.6 \pm 2.8 & (\text{Serpukhov [18]}). \end{cases} \quad (9.12)$$

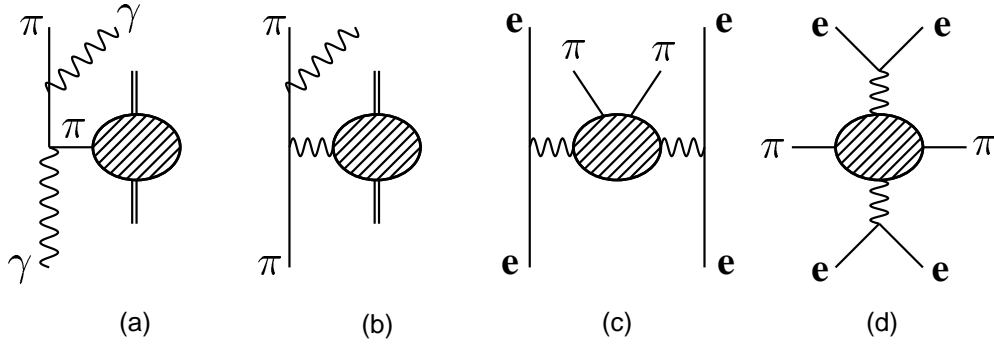


Figure 12: Compton scattering  $\gamma\pi \rightarrow \gamma\pi$  from the charged pion has been performed both via pion–photon production (a) and via radiative pion scattering (b) from a heavy target. Figures (c) and (d) show photon annihilation  $\gamma\gamma \rightarrow \pi\pi$  processes. The double lines denote nucleons.

Relaxing the constraint  $(\alpha + \beta)^C = 0$ , the Serpukhov data yield [35]

$$\begin{aligned} (\alpha + \beta)^C &= 1.4 \pm 3.1 \text{ (stat.)} \pm 2.5 \text{ (sys.)} , \\ (\alpha - \beta)^C &= 15.6 \pm 6.4 \text{ (stat.)} \pm 4.4 \text{ (sys.)} , \end{aligned} \quad (9.13)$$

where we have evaluated  $(\alpha - \beta)^C$  from  $\bar{\beta}_\pi$  and  $(\alpha + \beta)^C$  as given in Ref. [35], adding the errors in quadrature.

The amplitude  $\gamma\gamma \rightarrow \pi^+\pi^-$  at low energies is mainly sensitive to  $S$ -wave scattering. In Ref. [36] unitarized  $S$ -wave amplitudes have been constructed which contain  $(\alpha - \beta)^C$  as an adjustable parameter. A fit to Mark II data [10] gives

$$(\alpha - \beta)^C = 4.8 \pm 1.0 . \quad (9.14)$$

The result (9.14) contradicts the Serpukhov analysis Eq. (9.12). Taking into account also  $D$ -waves, Kaloshin et al. [37] find

$$(\alpha + \beta)^C = \begin{cases} 0.22 \pm 0.06 & \text{( Mark II [10] )} \\ 0.30 \pm 0.04 & \text{( CELLO [38] )} . \end{cases} \quad (9.15)$$

A detailed analysis of the same data has also been performed in [39]. The authors conclude that the errors quoted in Eq. (9.15) are underestimated, see also Ref. [40]. By reanalyzing the present data on the angular distribution of the  $\gamma\gamma \rightarrow \pi^+\pi^-$  reaction with using of the unitary model for helicity 2 amplitudes, Kaloshin et al. [41] find

$$(\alpha + \beta)^C = \begin{cases} 0.22 \pm 0.07 \text{ (stat.)} \pm 0.04 \text{ (sys.)} & \text{( Mark II [10] )} \\ 0.33 \pm 0.06 \text{ (stat.)} \pm 0.01 \text{ (sys.)} & \text{( CELLO [38] )} . \end{cases} \quad (9.16)$$

(We have taken into account that the definition of the polarizability in Refs. [36,37,41] is  $4\pi$  larger than the one used here).

Comparing with the data, the two-loop result for  $(\alpha + \beta)^C$  agrees within the error bars with the one found by Kaloshin et al. [37,41] (note the remark after Eq. (9.15))

and also with the data from Serpukhov [35]. The value for  $(\alpha - \beta)^C$  agrees within  $1\frac{1}{2}$  standard deviation with the measurement done at Lebedev [17] and also with the data analysis using unitarized S-waves in [36], however, appears to be inconsistent with the value quoted in [18].

For a more detailed discussion of the issues considered in this section, we refer the reader to Ref. [42]. In the following we shortly comment on the relation between the polarizabilities and the crossed channel reaction  $\gamma\gamma \rightarrow \pi^+\pi^-$ .

#### 9.4 Pion polarizabilities from $\gamma\gamma \rightarrow \pi^+\pi^-$ data

One may attempt to extract the polarizabilities from  $\gamma\gamma \rightarrow \pi^+\pi^-$  data in the following manner [11]. Our chiral representation at  $\mathcal{O}(p^6)$  contains three new low-energy constants  $h_{\pm}^{r,c}, h_s^{r,c}$ . The two parameters  $h_{\pm}^{r,c}$  may be replaced by the polarizabilities  $(\alpha \mp \beta)^C$ , whereas  $h_s^{r,c}$  may be determined e.g. from resonance exchange. In Fig. 13 we have plotted the  $\gamma\gamma \rightarrow \pi^+\pi^-$  cross section for a fixed value  $(\alpha + \beta)^C = 0.31$  and a fixed value  $h_s^{r,c} = -0.15$ , varying  $(\alpha - \beta)^C$  between 2.21 and 8.84. The sensitivity of the cross section to a change in  $(\alpha + \beta)^C$  is even weaker. Even a 100% change in  $(\alpha \pm \beta)^C$  is also consistent with the low-energy data. See also Fig. 9 in Ref. [11].

On the other hand by choosing a value for E and  $\sigma$  one may extract for a given value  $h_s^{r,c}$  the relation between  $(\alpha - \beta)^C$  and  $(\alpha + \beta)^C$ . This is plotted in Fig. 14 for different values of  $h_s^{r,c}$ , where one can see that the slope of  $(\alpha - \beta)^C$  is small and also changes in  $h_s^{r,c}$  do not affect  $(\alpha - \beta)^C$  significantly. We note that the sensitivity of  $(\alpha - \beta)^C$  due to variation in  $\sigma$  or in the low-energy couplings  $\bar{l}_i$  is very high. A one percent change e.g. in the cross section induces a 12% change in  $(\alpha - \beta)^C$ .

We confirm the statement [11] that, using the chiral representation of the  $\gamma\gamma \rightarrow \pi^+\pi^-$  amplitude as an interpolation, the statistical uncertainty of the present low-energy data as well as the uncertainties in the low-energy couplings do not allow one to pin down the charged pion polarizabilities to a reasonable accuracy. The same is true in the neutral channel [9, 11, 43].

## 10 Summary and conclusions

- (i) We use  $SU(2) \times SU(2) \times U(1)$  chiral perturbation theory to investigate the  $\gamma\gamma \rightarrow \pi^+\pi^-$  process up to two loops. We found that far more than 100 different diagrams contribute at  $\mathcal{O}(p^6)$ . Among these are genuine two-loop diagrams that cannot be represented as products of one-loop contributions (box, vertex, acnode and sunset). We find it important to take these diagrams into account, because they contribute substantially even near the threshold. The three new low-energy constants appearing at  $\mathcal{O}(p^6)$  have been estimated via resonance saturation by including vector- and axial-vector mesons ( $J^{PC} = 1^{--}, 1^{+-}, 1^{++}$ ).
- (ii) The one-loop approximation of the amplitude reproduces the available data on charged pion pair production from the MARK II experiment remarkably well. The corrections at  $\mathcal{O}(p^6)$  induce further small changes in the cross section, that then agrees rather well with the dispersion theoretic calculations [11, 12] at and also substantially above the threshold region. The enhancement (suppression) of the cross

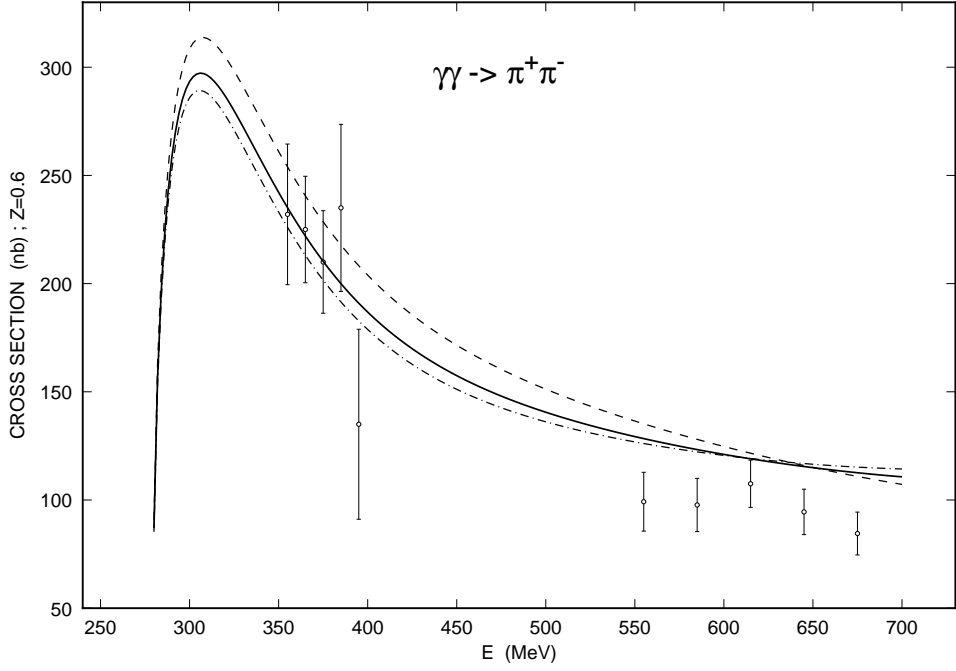


Figure 13: The two-loop result for the  $\gamma\gamma \rightarrow \pi^+\pi^-$  cross section parametrized through the polarizabilities. We set  $(\alpha+\beta)^c = 0.31$  and  $h_s^{r;c} = -0.15$ , varying  $(\alpha-\beta)^c$  between  $(\alpha-\beta)^c = 2.21$  (dash-dotted line) and  $(\alpha-\beta)^c = 8.84$  (dashed line). The solid line corresponds to  $(\alpha-\beta)^c = 4.42$ .

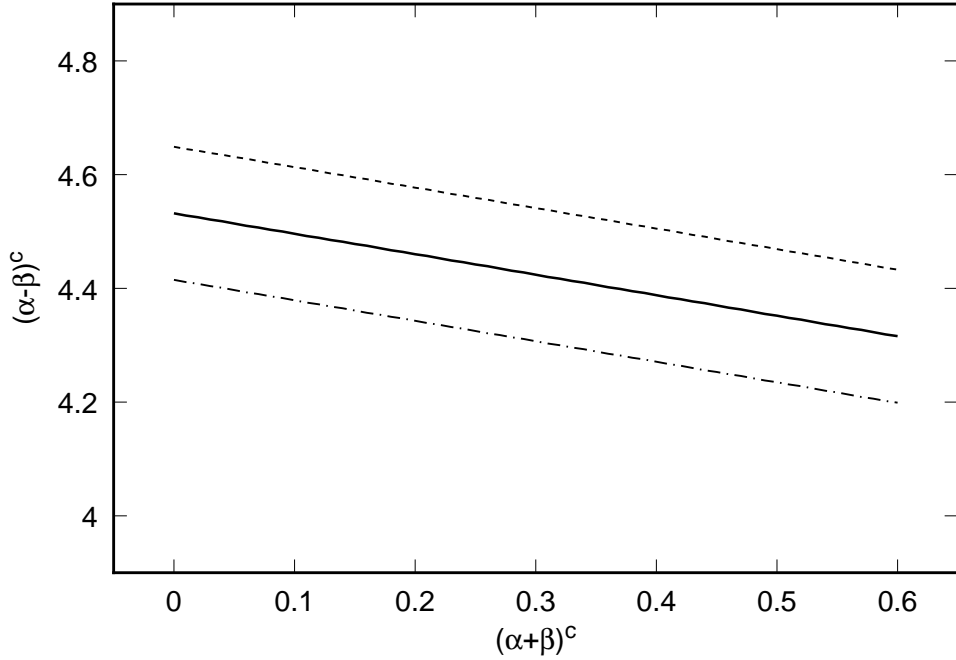


Figure 14: Relation between  $(\alpha+\beta)^c$  and  $(\alpha-\beta)^c$  by fixing a point in the  $\sigma$ - $E$ -plane ( $E=346$  MeV,  $\sigma=223.42$  nb), and for different values of  $h_s^{r;c}$ . The solid line corresponds to the central value  $h_s^{r;c} = -0.15$  whereas the upper (lower) line is evaluated with  $h_s^{r;c} = -0.55(0.25)$ .

section very close to threshold (above  $E = 350$  MeV) is mainly due to  $\pi\pi$  rescattering and renormalization of the pion decay constant, see Fig. 9. The couplings  $h_{\pm}^{r,c}$  and  $h_s^{r,c}$  contribute with a negligible amount below  $E = 450$  MeV, they become, however, more important at higher energies.

- (iii) The cross section for  $\gamma\pi^{\pm} \rightarrow \gamma\pi^{\pm}$  is fully dominated by the Born terms. One- and two-loop corrections are completely negligible in this case.
- (iv) The expansion of the amplitude at the Compton threshold in powers of the photon energies allows one to extract the pion polarizabilities in powers of the quark masses. We note that the sum of the polarizabilities is positive, as is suggested by the unsubtracted forward dispersion relation (see e.g. [24]). Furthermore,  $(\alpha + \beta)^C$  vanishes in the chiral limit  $m_u = m_d = 0$ . The chiral expansion of the polarizabilities contain chiral logarithms  $\sim M_{\pi} \ln^2 M_{\pi}$  and  $\sim M_{\pi} \ln M_{\pi}$  which are suppressed by small Clebsch–Gordan coefficients. Nevertheless their effect on the pion polarizabilities is substantial. The effect of the low-energy constants  $h_{\pm}^{r,c}$  on the pion polarizability is large ( $\sim 50\%$  of the two-loop result). It is therefore essential to make additional efforts in estimating the  $\mathcal{O}(p^6)$  low-energy constants in order to reduce the theoretical uncertainties in the polarizabilities.
- (v) We comment on the comparison of the chiral predictions for  $(\alpha \pm \beta)^C$  with the data.
  - Our result  $(\alpha - \beta)^C = 4.4 \pm 1.0$  includes the leading and next-to-leading order terms. It agrees within  $1\frac{1}{2}$  standard deviation with the result  $40 \pm 24$  found at Lebedev [17]. On the other hand, it is inconsistent with the value  $13.6 \pm 2.8$  determined at Serpukhov [18].
  - The analysis done by Kaloshin et al. [36,37,41] for  $(\alpha \pm \beta)^C$  agrees within the error bars with the chiral predictions. Beware, however, the remark after Eq. (9.15).
  - The value  $(\alpha + \beta)^C = 0.3 \pm 0.1$  includes the leading order term, generated by two-loop graphs. It is in good agreement with the result  $(\alpha + \beta)^C = 0.39 \pm 0.04$  [29], obtained from a forward angle dispersion sum rule based on the optical theorem and evaluated in a model dependent way. (Note, e.g., that the lagrangian used in this model is not chiral invariant.)
- (vi) In principle, the chiral representation of the  $\gamma\gamma \rightarrow \pi^+\pi^-$  amplitude may be used as an interpolation to extract the pion polarizabilities from the low energy data. However, the cross section is rather insensitive to  $(\alpha \pm \beta)^C$ , and a reliable determination seems not to be possible in this manner [11,12].
- (vii) In order to clarify the experimental situation, new experiments to determine the pion polarizabilities have been planned at Fermilab (E781 SELEX), Frascati (DAΦNE), Grenoble (Graal facility) and at Mainz (MAMI). We refer the reader to the section on hadron polarizabilities in Ref. [20] for details.

## Acknowledgments

I thank Jürg Gasser for his help and advice throughout this work and for reading this manuscript carefully, Mikko Sainio for useful discussions about numerical issues and finally Hagen Eck and Sepp Kueblbeck for the update of *FeynArts* to handle CHPT, too.

## A One-loop integrals

We use dimensional regularization and set

$$\omega = \frac{d}{2} - 2 \leq 0. \quad (\text{A.1})$$

Physical results will be obtained by letting  $d \rightarrow 4$  ( $\omega \rightarrow 0$ ).

### A.1 The integrals $F_m(z)$

Most of the two-loop graphs can be expressed through the one-loop function  $F_m(z)$ . We use the following representation :

$$\int \frac{d^d l}{i(2\pi)^d} \frac{1}{[z - l^2]^m} = F_m(z). \quad (\text{A.2})$$

The  $F_m$  satisfy the recursion relation

$$z F_m(z) = \frac{m-3-\omega}{m-1} F_{m-1}(z) \quad , \quad m \geq 2, \quad (\text{A.3})$$

and are given by

$$F_m(z) = (4\pi)^{-2-\omega} \frac{\Gamma(m-2-\omega)}{\Gamma(m)} z^{\omega+2-m} \quad , \quad m \geq 1. \quad (\text{A.4})$$

### A.2 The loop integrals $J(s)$ , $\bar{J}(s)$ and $\bar{\bar{J}}(s)$

We denote by  $J(s)$  the standard one-loop integral ( $s \doteq p^2$ )

$$J(s) = \int \frac{d^d l}{i(2\pi)^d} \frac{1}{M^2 - l^2} \frac{1}{M^2 - (l+p)^2}. \quad (\text{A.5})$$

After Feynman-parametrization one gets

$$\begin{aligned} J(s) &= \int_0^1 dx F_2(z), \\ z &= M^2 - sx(1-x). \end{aligned} \quad (\text{A.6})$$

$J(s)$  is real analytic in the complex  $s$ -plane, cut along the positive real axis for  $\text{Res} > 4M^2$ . The pole at  $\omega = 0$  may be isolated by writing

$$J(s) = J(0) + \bar{J}(s), \quad (\text{A.7})$$

where  $J(0)$  contains the pole,

$$J(0) = F_2(M^2) = -\frac{1}{16\pi^2} \frac{1}{\omega} + \mathcal{O}(1) \quad ; \quad \omega \rightarrow 0, \quad (\text{A.8})$$

and  $\bar{J}(s)$  is the finite loop integral

$$\bar{J}(s) = -\frac{1}{16\pi^2} \int_0^1 dx \ln \left( 1 - \frac{s}{M^2} x(1-x) \right). \quad (\text{A.9})$$

At small  $s$ , after expanding the integrand one finds

$$\bar{J}(s) = \frac{1}{16\pi^2} \sum_{n=1}^{\infty} \left( \frac{s}{M^2} \right)^n \frac{(n!)^2}{n(2n+1)!}. \quad (\text{A.10})$$

For  $s > 4M^2$  the logarithm generates an imaginary part

$$\begin{aligned} \mathcal{I}m \bar{J}(s) &= \frac{\beta(s)}{16\pi}, \quad s > 4M^2, \\ \beta(s) &= \sqrt{1 - \frac{4M^2}{s}}. \end{aligned} \quad (\text{A.11})$$

Explicitly,

$$16\pi^2 \bar{J}(s) = \begin{cases} \beta \left( \ln \frac{1-\beta}{1+\beta} + i\pi \right) + 2 & ; \quad 4M^2 \leq s \\ 2 - 2 \left( \frac{4M^2-s}{s} \right)^{\frac{1}{2}} \arctan \left( \frac{s}{4M^2-s} \right)^{\frac{1}{2}} & ; \quad 0 \leq s \leq 4M^2 \\ \beta \ln \frac{\beta-1}{\beta+1} + 2 & ; \quad s \leq 0. \end{cases} \quad (\text{A.12})$$

In the text we also need

$$\begin{aligned} \bar{\bar{J}}(s) &= \bar{J}(s) - s\bar{J}'(0), \\ s\bar{J}'(0) &= \frac{1}{96\pi^2} \frac{s}{M^2}. \end{aligned} \quad (\text{A.13})$$

### A.3 The loop integrals $\bar{G}(s)$ , $\bar{\bar{G}}(s)$ and $\bar{H}(s)$

The integral  $\bar{G}(s)$  may be obtained from the tensorial integral

$$\int \frac{d^d l}{i(2\pi)^d} \left[ \frac{(2l+q_1)^\mu (2l-q_2)^\nu}{D_0} + g^{\mu\nu} \right] \frac{1}{D_1 D_2} = \left( g^{\mu\nu} - \frac{2}{s} q_2^\mu q_1^\nu \right) \bar{G}(s), \quad (\text{A.14})$$

$$D_0 = M^2 - l^2 \quad ; \quad D_1 = M^2 - (l+q_1)^2 \quad ; \quad D_2 = M^2 - (l-q_2)^2,$$

where

$$\bar{G}(s) = -\frac{1}{16\pi^2} \left\{ 1 + \frac{2M^2}{s} \int_0^1 \frac{dx}{x} \ln \left( 1 - \frac{s}{M^2} x(1-x) \right) \right\}. \quad (\text{A.15})$$

$\bar{G}$  is analytic in the complex  $s$ -plane, cut along the positive real axis for  $\mathcal{R}es \geq 4M^2$ . At small  $s$ , after expanding the integrand one finds

$$\bar{G}(s) = \frac{1}{16\pi^2} \sum_{n=1}^{\infty} \left( \frac{s}{M^2} \right)^n \frac{(n!)^2}{(n+1)(2n+1)!}. \quad (\text{A.16})$$

For  $s > 4M^2$  the logarithm generates an imaginary part

$$\begin{aligned} \mathcal{I}m \bar{G}(s) &= \frac{M^2}{8s\pi} \ln \left\{ \frac{1 + \beta(s)}{1 - \beta(s)} \right\} , \quad s > 4M^2, \\ \beta(s) &= \sqrt{1 - \frac{4M^2}{s}} . \end{aligned} \quad (\text{A.17})$$

Use of the Spence function  $Li_2$ , especially of

$$\begin{aligned} Li_2(y) + Li_2\left(\frac{-y}{1-y}\right) &= -\frac{1}{2} \ln^2(1-y) , \\ Li_2(y) &= -\int_0^y \frac{dx}{x} \ln(1-x) , \end{aligned} \quad (\text{A.18})$$

gives

$$-16\pi^2 \bar{G}(s) = \begin{cases} 1 + \frac{M^2}{s} \left( \ln \frac{1-\beta}{1+\beta} + i\pi \right)^2 & ; \quad 4M^2 \leq s \\ 1 - \frac{4M^2}{s} \arctan^2\left(\frac{s}{4M^2-s}\right)^{\frac{1}{2}} & ; \quad 0 \leq s \leq 4M^2 \\ 1 + \frac{M^2}{s} \ln^2 \frac{\beta-1}{\beta+1} & ; \quad s \leq 0 . \end{cases} \quad (\text{A.19})$$

In the text we also need

$$\begin{aligned} \bar{\bar{G}}(s) &= \bar{G}(s) - s\bar{G}'(0) , \\ s\bar{G}'(0) &= \frac{1}{192\pi^2} \frac{s}{M^2} . \end{aligned} \quad (\text{A.20})$$

The loop function  $\bar{H}(s)$  is defined in terms of  $\bar{G}$  and  $\bar{J}$ ,

$$\bar{H}(s) = (s - 10M^2)\bar{J}(s) + 6M^2\bar{G}(s) . \quad (\text{A.21})$$

## References

- [1] S. Weinberg, *Physica A* 96 (1979) 327.
- [2] J. Gasser and H. Leutwyler, *Ann. Phys. (N.Y.)* 158 (1984) 142.
- [3] J. Gasser and H. Leutwyler, *Nucl. Phys. B* 250 (1985) 465.
- [4] H. Leutwyler, *Ann. Phys. (N.Y.)* 235 (1994) 165.
- [5] For recent reviews on CHPT see e.g.  
H. Leutwyler, *Chiral effective lagrangians*, *Lecture Notes in Physics*, vol. 396, eds. H. Mitter and H. Gausterer, Springer-Verlag (Berlin, 1991);  
*Nonperturbative methods*, *Proc. XXVI Int. Conf. on High Energy Physics*, Dallas, 1992, ed. J.R. Sanford, *AIP Conf. Proc. No. 272* (AIP, New York, 1993) p. 185;  
U.G. Meißner, *Rep. Prog. Phys.* 56 (1993) 903;  
A. Pich, *Lectures given at the V Mexican School of Particles and Fields*, Guanajuato, México, December 1992, preprint CERN-Th.6978/93 (hep-ph/9308351);  
A. Pich, *Chiral Perturbation Theory*, *Rept. Prog. Phys.* 58 (1995) 563;



- G. Ecker, Chiral perturbation theory, in: Quantitative Particle Physics: Cargèse 1992, eds. M Lévy et al., Plenum Publ. Co. (New York, 1993);  
 J.F. Donoghue, E. Golowich and B.R. Holstein, "Dynamics of the Standard Model" (1992), Cambridge University Press, Cambridge.
- [6] J. Bijnens and F. Cornet, Nucl. Phys. B 296 (1988) 557.
- [7] J.F. Donoghue, B.R. Holstein and Y.C. Lin, Phys. Rev. D 37 (1988) 2423.
- [8] Crystal Ball Collab., H. Marsiske et al., Phys. Rev. D 41 (1990) 3324.
- [9] S. Bellucci, J. Gasser and M.E. Sainio, Nucl. Phys. B 423 (1994) 80; *ibid.* B 431 (1994) 413 (erratum).
- [10] Mark II Collab., J. Boyer et al., Phys. Rev. D 42 (1990) 1350.
- [11] J.F. Donoghue and B.R. Holstein, Phys. Rev. D 48 (1993) 137.
- [12] M.R. Pennington, in Ref. [13], p. 531.
- [13] L. Maiani, G. Pancheri and N. Paver, eds., The Second DAΦNE Physics Handbook (INFN, Frascati, 1995).
- [14] M.V. Terent'ev, Sov. J. Nucl. Phys. 16 (1973) 87.
- [15] J.F. Donoghue and B.R. Holstein, Phys. Rev. D 40 (1989) 2378.
- [16] B.R. Holstein, Comm. Nucl. Part. Phys. 19 (1990) 221.
- [17] T.A. Aibergenov et al., Czech. J. Phys. B 36 (1986) 948.
- [18] Yu.M. Antipov et al., Phys. Lett. 121B (1983) 445; Z. Phys. C24 (1984) 39.
- [19] R. Baldini and S. Bellucci, Pion (Kaon) and Sigma polarizabilities, in Ref. [20], p. 177.
- [20] Chiral Dynamics: Theory and Experiment, Proceedings of the Workshop held at MIT, Cambridge, MA, USA, 25–29 July 1994, eds. A.M. Bernstein and B.R. Holstein, Springer–Verlag (Berlin 1995).
- [21] Ll. Ametller, J. Bijnens, A. Bramon and F. Cornet, Phys. Lett. B 276 (1992) 185.
- [22] H.W. Fearing and S. Scherer, Phys. Rev. D 53 (1996) 315.
- [23] S. Kueblbeck, H. Eck, Generating Feynman Graphs and Amplitudes with *FeynArts*, Manual and *Mathematica* source via FTP from mathsource.wri.com, Version 1.0.
- [24] U. Bürgi, Ph.D. thesis, University of Berne (1996).
- [25] U. Bürgi, J. Gasser and M.E. Sainio, in preparation.
- [26] J. Bijnens, G. Colangelo and J. Gasser, Nucl. Phys. B 427 (1994) 427.
- [27] J. Bijnens et al., in preparation.

- [28] G. Ecker, J. Gasser, A. Pich and E. de Rafael, Nucl. Phys. B 321 (1989) 311;  
G. Ecker et al., Phys. Lett B 223 (1989) 425;  
G. Ecker, A. Pich and E. de Rafael, Phys. Lett. B 237 (1990) 481.
- [29] V.A. Petrun'kin, Sov. J. Part. Nucl. 12 (1981) 278.
- [30] A.E. Kaloshin and V.V. Serebryakov, Z. Phys. C 32 (1986) 279.
- [31] P. Ko, Phys. Rev. D 41 (1990) 1531.
- [32] D. Babusci et al., Phys. Lett. B 314 (1993) 112.
- [33] R.V. Kowalewski et al., Phys. Rev. D 29 (1984) 1000.
- [34] For reviews on polarizabilities see e.g.  
V.A. Petrun'kin, in Ref. [29];  
J.L. Friar, *in* Proc. Workshop on Electron–Nucleus Scattering, Marciana Marina, 7–15 June 1988, eds. A. Fabrocini et al. (World Scientific, Singapore, 1989) p. 3;  
B.R. Holstein, in Ref. [16];  
M.A. Moinester, *in* Proc. 4th Conf. on the Intersections Between Particle and Nuclear Physics, Tucson, Arizona, May 24–29, 1991, AIP Conf. Proc. No. 243, ed. W.T.H. Van Oers (AIP, New York, 1992), p. 553.
- [35] Yu.M. Antipov et al., Z. Phys. C 26 (1985) 495.
- [36] A.E. Kaloshin and V.V. Serebryakov, Z. Phys. C 64 (1994) 689.
- [37] A.E. Kaloshin, V.M. Persikov and V.V. Serebryakov, Phys. Atom. Nucl. 57 (1994) 2207.
- [38] The CELLO collaboration, H.–J. Behrend et al., Z. Phys. C 56 (1992) 381.
- [39] D. Morgan and M.R. Pennington, Z. Phys. C 48 (1990) 623.
- [40] J. Portolés and M.R. Pennington, in Ref. [13], p. 579; M.R. Pennington, talk given at the working group on polarizabilities, see Ref. [20].
- [41] A.E. Kaloshin, V.M. Persikov and V.V. Serebryakov, preprint ISU–IAP.Th95–01 (hep–ph/9504261).
- [42] U. Bürgi, preprint BUTP–96/01; (hep–ph/9602421).
- [43] J. Gasser, Low–energy photon–photon collisions to two–loop order, in Ref. [20], p. 139.